HHS Public Access

Author manuscript

Nat Med. Author manuscript; available in PMC 2017 August 24.

Published in final edited form as:

Nat Med. 2016 May ; 22(5): 506–515. doi:10.1038/nm.4072.

Epithelial calcineurin controls microbiota-dependent intestinal tumor development

Kenneth Peuker[1,2,18], **Stefanie Muff**[1,18], **Jun Wang**[3,4], **Sven Künzel**[3,4], **Esther Bosse**[1], **Yvonne Zeissig**[5,6], **Giuseppina Luzzi**[1,2], **Marijana Basic**[7], **Anne Strigli**[2], **Andrea Ulbricht**[1], **Arthur Kaser**[8], **Alexander Arlt**[1], **Triantafyllos Chavakis**[9,10], **Gijs R van den Brink**[11,12], **Clemens Schafmayer**[13], **Jan-Hendrik Egberts**[13], **Thomas Becker**[13], **Marco E Bianchi**[14], **André Bleich**[7], **Christoph Röcken**[15], **Jochen Hampe**[1,16], **Stefan Schreiber**[1], **John F Baines**[3,4], **Richard S Blumberg**[17,19], and **Sebastian Zeissig**[1,2,16,17,19]

[1]Department of Internal Medicine I, University Medical Center Schleswig-Holstein, Kiel, Germany [2]Center for Regenerative Therapies, Technical University Dresden, Dresden, Germany [3]Max Planck Institute for Evolutionary Biology, Plön, Germany [4]Institute for Experimental Medicine, Christian-Albrechts University of Kiel, Kiel, Germany [5]Department of General Pediatrics, University Medical Center Schleswig-Holstein, Kiel, Germany [6]Department of Pediatrics, University Medical Center Dresden, Technical University Dresden, Dresden, Germany [7]Institute for Laboratory Animal Science and Central Animal Facility, Hannover Medical School, Hannover, Germany [8]Division of Gastroenterology, Addenbrooke Hospital, University of Cambridge, Cambridge, UK [9]Department of Clinical Pathobiochemistry, Faculty of Medicine, Technical University Dresden, Dresden, Germany [10]Institute of Clinical Chemistry and Laboratory Medicine, Faculty of Medicine, Technical University Dresden, Dresden, Germany [11]Tytgat Institute for Liver and Intestinal Research, Academic Medical Center, Amsterdam, the Netherlands [12]Department of Gastroenterology and Hepatology, Academic Medical Center, Amsterdam, the Netherlands [13]Department of General Surgery and Thoracic Surgery, University Hospital Schleswig-Holstein, Kiel, Germany [14]San Raffaele University and Scientific Institute, Milan, Italy [15]Institute of Pathology, University Medical Center Schleswig-Holstein, Kiel, Germany [16]Department of Medicine I, University Medical Center Dresden, Technical University Dresden, Dresden, Germany

Correspondence should be addressed to S.Z. (sebastian.zeissig@uniklinikum-dresden.de) or R.S.B. (rblumberg@partners.org).
[18]These authors contributed equally to this work.
[19]These authors jointly directed this work.

Note: Any Supplementary Information and Source Data files are available in the online version of the paper.

AUTHOR CONTRIBUTIONS

K.P., S.M., E.B., G.L. and A.S. developed and analyzed the described mouse models and performed *in vivo* and *in vitro* studies. J.W., S.K. and J.F.B. performed microbiota analyses and provided GF mice. M.B. and A.B. provided GF mice. A.U. contributed to EGF and VEGF signaling studies and to the generation of adenovirus. Y.Z. and C.R. performed histopathological analyses. A.K. contributed to stem cell analyses. G.R.v.d.B. provided RAGE-KO tissues. T.C. and M.E.B. contributed to HMGB1 studies. J.H., C.S., J.-H.E. and T.B. collected and provided CRC tissues. A.A. and S.S. contributed to the coordination of experimental studies. R.S.B. and S.Z. designed the study, coordinated the experimental work and wrote the manuscript with input from the coauthors. All authors discussed the results and commented on the manuscript. S.Z. and R.S.B. contributed equally to this work and are co-corresponding authors.

COMPETING FINANCIAL INTERESTS

The authors declare no competing financial interests.

[17]Division of Gastroenterology, Hepatology and Endoscopy, Brigham and Women's Hospital, Harvard Medical School, Boston, Massachusetts, USA

Abstract

Inflammation-associated pathways are active in intestinal epithelial cells (IECs) and contribute to the pathogenesis of colorectal cancer (CRC). Calcineurin, a phosphatase required for the activation of the nuclear factor of activated T cells (NFAT) family of transcription factors, shows increased expression in CRC. We therefore investigated the role of calcineurin in intestinal tumor development. We demonstrate that calcineurin and NFAT factors are constitutively expressed by primary IECs and selectively activated in intestinal tumors as a result of impaired stratification of the tumor-associated microbiota and toll-like receptor signaling. Epithelial calcineurin supports the survival and proliferation of cancer stem cells in an NFAT-dependent manner and promotes the development of intestinal tumors in mice. Moreover, somatic mutations that have been identified in human CRC are associated with constitutive activation of calcineurin, whereas nuclear translocation of NFAT is associated with increased death from CRC. These findings highlight an epithelial cell–intrinsic pathway that integrates signals derived from the commensal microbiota to promote intestinal tumor development.

Intestinal inflammation as observed in inflammatory bowel disease (IBD) is a risk factor for the development of CRC[1]. Increasing evidence suggests that inflammation-associated pathways also contribute to CRC development in the absence of clinically overt intestinal inflammation[1]. Thus, signaling pathways with central roles in myeloid and lymphoid cells, such as those associated with signal transducer and activator of transcription 3 (STAT3) and nuclear factor (NF)-κB, are also active in the transformed intestinal epithelium and promote tumor development[2–6].

Calcineurin is a phosphatase with central functions in immunity, many of which are elicited by dephosphorylation and activation of NFAT transcription factors[7] (which we collectively refer to as NFAT). In accordance with an important role of calcineurin in immunity, calcineurin inhibitors are widely used to suppress undesired immune responses, particularly in solid organ transplantation. The pharmacological inhibition of calcineurin therefore leads to an increase in the incidence of solid cancers including CRC, presumably as a consequence of impaired calcineurin-dependent tumor immunosurveillance[8,9]. In contrast to these observations *in vivo*, the blockade of calcineurin and NFAT in isolated CRC cell lines *in vitro* inhibits, rather than promotes, CRC cell growth[10–13], thus raising the question of whether epithelial calcineurin and NFAT exhibit cell-intrinsic oncogenic roles in CRC. Here we show that calcineurin and NFAT are constitutively expressed by IECs and undergo toll-like receptor (TLR)-induced activation in response to impaired stratification of the tumor-associated microbiota and increased TLR expression by tumor cells. Epithelial calcineurin promotes intestinal tumor development through the regulation of cancer stem cell function in mice, and its activation in human CRC is associated with increased death from CRC.

RESULTS

Epithelial calcineurin promotes intestinal tumor development

To investigate the role of epithelial calcineurin in intestinal tumor development, we generated mice with an IEC-specific deletion of the regulatory B1 subunit of calcineurin (Cnb1; encoded by *Ppp3r1*), which is required for calcineurin activation, using *loxP*-flanked ('floxed') alleles of *Ppp3r1* and Cre-mediated deletion (villin-*Cre*;*Ppp3r1*$^{fl/fl}$ mice; hereafter referred to as Cnb1$^{\Delta IEC}$ mice). Cnb1$^{\Delta IEC}$ mice were crossed with *Apc*$^{Min/+}$ mice[14], which have one mutated allele of the adenomatosis polyposis coli (*Apc*) gene and are a model for genetically induced intestinal tumors. The IEC-specific loss of Cnb1 (Supplementary Fig. 1a,b) did not affect epithelial differentiation (Supplementary Fig. 1c,d), but it was associated with reduced intestinal tumor multiplicity and size, as compared to villin-*Cre*–negative wild-type (WT) littermates (*Ppp3r1*$^{fl/fl}$;*Apc*$^{Min/+}$ mice, hereafter referred to as Cnb1^{WT};*Apc*$^{Min/+}$ mice; Fig. 1a,b and Supplementary Fig. 1e). Early-stage lesions, such as microadenomas, were also reduced in Cnb1$^{\Delta IEC}$;*Apc*$^{Min/+}$ mice, consistent with calcineurin-dependent regulation of tumor initiation (Supplementary Fig. 1f). Furthermore, deletion of *Ppp3r1* in established tumors of 12-week-old villin-CreER^{T2};*Ppp3r1*$^{fl/fl}$;*Apc*$^{Min/+}$—a model with tamoxifen-inducible, IEC-specific deletion of *Ppp3r1*, which we refer to as Cnb1$^{ind\Delta IEC}$ mice—was associated with decreased tumor size, in accordance with calcineurin-dependent tumor growth (Fig. 1c and Supplementary Fig. 1g). Tumor multiplicity and size were also reduced in Cnb1$^{\Delta IEC}$ mice treated with colitis-inducing dextran sulfate sodium (DSS) in conjunction with the carcinogen azoxymethane (AOM) (Fig. 1d,e and Supplementary Fig. 1h), despite an increase in body weight loss and an increase in the disease activity index (Supplementary Fig. 1i–k). Thus, the tumor-promoting effects of epithelial calcineurin extend to the colon and to colitis-associated CRC. These results demonstrate that epithelial calcineurin supports intestinal tumor initiation and growth in mice.

We next addressed the mechanisms underlying calcineurin-dependent tumor development. Because tumorigenesis in *Apc*$^{Min/+}$ mice recapitulates central steps of early intestinal tumor development in humans and occurs in the absence of clinically overt intestinal inflammation, similar to what is observed in the majority of human CRCs, we focused on the *Apc*$^{Min/+}$ model for subsequent mechanistic studies. Epithelial proliferation was reduced and apoptosis was increased in Cnb1-deficient adenomas and microadenomas, whereas senescence was not observed (Fig. 1f,g, Supplementary Fig. 2a,b and data not shown (K.P.)). Cnb1-dependent regulation of proliferation and apoptosis was not observed in normal IECs of Cnb1$^{\Delta IEC}$;*Apc*^{WT} mice and was thus specific for the tumor-associated epithelium (Supplementary Fig. 2c,d). These data suggest that calcineurin supports intestinal tumor development through promotion of epithelial proliferation and inhibition of apoptosis.

Tumor-promoting effects of calcineurin are mediated by NFAT

To identify the molecular mediators of calcineurin-dependent tumor growth, we investigated the role of the NFAT family of transcription factors, of which NFATc1, NFATc2, NFATc3 and NFATc4 are dependent on calcineurin for dephosphorylation and nuclear translocation[7]. NFATc3 was consistently expressed in primary human CRC and CRC cell lines, whereas other calcineurin-dependent NFAT members showed weak and inconsistent expression CRC

cells, with occasional detection of NFATc1 in tumor-infiltrating cells but not in epithelial cells (Fig. 2a,b). In mice, normal small intestinal epithelium showed exclusive expression of NFATc3 (Supplementary Fig. 3a and data not shown (K.P.)). *Apc*$^{Min/+}$ tumors demonstrated increased *Nfatc3* expression, as compared to normal mucosa, but weak expression of *Nfatc1*, *Nfatc2* and *Nfatc4* (Fig. 2c,d and Supplementary Fig. 3b). Consistent with calcineurin-dependent regulation of apoptosis and proliferation in tumors but not in normal epithelium (Fig. 1f,g and Supplementary Fig. 2c,d), NFATc3 was cytoplasmic in normal IECs but showed calcineurin-dependent nuclear translocation in *Apc*$^{Min/+}$ tumors (Fig. 2e). Thus, NFATc3 is constitutively expressed by IECs, whereas its calcineurin-dependent activation is specific to intestinal tumors.

To address whether NFATc3 promotes tumor development downstream of calcineurin, we investigated mice with an IEC-specific deletion of *Nfatc3* (villin-*Cre*;*Nfatc3*$^{fl/fl}$; hereafter referred to as *Nfatc3*$^{\Delta IEC}$ mice). Both in the *Apc*$^{Min/+}$ mice and in the AOM-DSS model, tumor size (Fig. 2f,g) and proliferation (Fig. 2h and Supplementary Fig. 3c) were reduced in *Nfatc3*$^{\Delta IEC}$ mice as compared to that in their WT littermates, whereas the severity of colitis in the AOM-DSS model was not affected (Supplementary Fig. 3d). Consistent with these observations, transduction of tumors with an adenoviral construct encoding calcineurin-independent, constitutively active NFATc3 (Ad-*NFATC3*^{CA}) increased tumor growth in Cnb1$^{\Delta IEC}$;*Apc*$^{Min/+}$ mice (Fig. 2i and Supplementary Fig. 3e,f). Ad-*NFATC3*^{CA} transduction did not further promote tumor growth in Cnb1^{WT};*Apc*$^{Min/+}$ mice (Fig. 2i), consistent with the idea that constitutive tumor-associated activation of NFATc3 occurs in the presence of functional calcineurin (Fig. 2e).

Because the reduction in tumor size was more pronounced in Cnb1$^{\Delta IEC}$ mice than in *Nfatc3*$^{\Delta IEC}$ mice (Figs. 1b,e and 2f,g) and because a reduction in tumor multiplicity was not observed in *Nfatc3*$^{\Delta IEC}$ mice (Supplementary Fig. 3g,h), we investigated the role of other NFAT factors in intestinal tumor development. Deletion of *Nfatc1* in intestinal epithelial cells (using villin-*Cre*;*Nfatc1*$^{fl/fl}$;*Apc*$^{Min/+}$ mice) did not affect tumor multiplicity or size, whereas tumor development in mice with a combined IEC-specific deletion of *Nfatc1* and *Nfatc3* was indistinguishable from that in *Nfatc3*$^{\Delta IEC}$ mice (Supplementary Fig. 3i and data not shown (K.P.)). Because a compensatory increase in *Nfatc2* expression was detected in tumors from *Nfatc3*$^{\Delta IEC}$ mice (Supplementary Fig. 3j), we considered the possibility that abrogation of NFAT-dependent tumor development may require the combined inhibition of all calcineurin-dependent NFAT factors to avoid escape mechanisms. We therefore treated *Apc*$^{Min/+}$ mice with adenoviruses expressing VIVIT (Ad-VIVIT; Supplementary Fig. 4a), a peptide (MAGPHPVIVITGPHEE) that interferes with calcineurin-dependent activation of NFAT[15]. Ad-VIVIT treatment resulted in reduced tumor size, multiplicity and proliferation, and it increased tumor apoptosis (Fig. 2j and Supplementary Fig. 4b,c)—findings that resembled observations in Cnb1$^{\Delta IEC}$;*Apc*$^{Min/+}$ mice. Together, these studies suggest that calcineurin promotes intestinal tumor development through the activation of NFAT. In contrast, calcineurin did not affect epithelial NF-κB and STAT3 signaling (Supplementary Results and Supplementary Fig. 5).

Microbiota-dependent activation of epithelial calcineurin

We next aimed to determine the factors responsible for the activation of calcineurin and NFAT in intestinal tumors. Mutations in *APC*, *TP53* (which encodes the tumor suppressor protein p53) and the *KRAS* oncogene contribute to human CRC development, and Ras, as well as mutant p53, can activate NFAT[16–18]. Furthermore, noncanonical Wnt signaling and growth factors can promote the activation of NFAT[19–22]. However, we did not find evidence for a role of canonical or noncanonical Wnt signaling, p53, Ras or growth factor signaling in the activation of tumor-associated calcineurin (Supplementary Results and Supplementary Figs. 6 and 7).

Recent work has revealed a central role of the microbiota, and its TLR-dependent recognition, in intestinal tumor development in humans[23–26] and rodents[27–32]. In the $Apc^{Min/+}$ model, TLR-induced Myd88 signaling in the nonhematopoietic compartment[30], and specifically in the IECs[33], regulates tumor growth through control of epithelial proliferation and apoptosis[30,32]. Accordingly, antibiotic treatment[34] and germ-free (GF) rederivation[28,31] inhibit intestinal tumor development in $Apc^{Min/+}$ mice. TLR agonists have been shown to activate calcineurin and NFAT in dendritic cells[35], so we investigated whether signaling by TLR2 and TLR4, the TLRs most strongly induced in $Apc^{Min/+}$ tumors (Supplementary Fig. 8a) and expressed by primary human CRC cells[36] and SW707 CRC cells (data not shown (K.P.)), promotes the activation of tumor-associated calcineurin. Stimulation of TLR4, and to a lesser extent TLR2, led to a sustained increase in intracellular Ca^{2+} (Fig. 3a), an increase in the DNA binding activity of NFAT (Fig. 3b), nuclear translocation of ectopically expressed NFATc3 fused to green fluorescent protein (NFATc3–GFP) (Fig. 3c) and NFAT-dependent transcription in human CRC cells (Fig. 3d). The TLR-induced increase in the DNA-binding activity of NFAT was inhibited by small hairpin RNA (shRNA)-mediated knockdown of *PPP3R1*, chelation of extracellular Ca^{2+} by EGTA, the use of Ca^{2+}-free medium, and chemical inhibition of calcium release–activated channels (CRACs) by 3,5-bis(trifluoromethyl)pyrazole (BTP) 2 and of phospholipase C by U73122 (Fig. 3e,f and Supplementary Fig. 8b). These results suggest that TLR stimulation promotes store-operated calcium entry, nuclear NFAT translocation and NFAT-dependent transcription in CRC cells.

Because TLR agonists can activate calcineurin and NFAT in CRC cells, we next assessed the role of TLR signaling in calcineurin-dependent tumor development. Exposure to lipopolysaccharide (LPS) increased the proliferation of human CRC cells in a calcineurin- and NFATc3-dependent manner (Fig. 3g). Similarly, LPS promoted the growth and proliferation of organoids from tumors of $Cnb1^{WT}$;$Apc^{Min/+}$ but not $Cnb1^{\Delta IEC}$;$Apc^{Min/+}$ mice (Fig. 3h and Supplementary Fig. 8c) through TLR4 (Supplementary Fig. 8d). We therefore investigated whether the microbiota and its recognition by TLRs are required for calcineurin-dependent tumor growth *in vivo*. To this end, $Apc^{Min/+}$ mice were either crossed with mice deficient in *Myd88* or treated with antibiotics (Supplementary Fig. 8e)—both of which are associated with decreased intestinal tumor growth in mice with a loss of functional APC[5,30,32,34]. *Myd88*-deficiency or antibiotic treatment (Supplementary Fig. 8f) prevented nuclear translocation of NFATc3 in $Apc^{Min/+}$ tumors (Fig. 4a) and reduced NFAT-dependent transcription in tumors from $Cnb1^{WT}$;$Apc^{Min/+}$ but not $Cnb1^{\Delta IEC}$;$Apc^{Min/+}$ mice

(Fig. 4b). Moreover, antibiotic treatment reduced tumor multiplicity and size in Cnb1^{WT};*Apc*$^{Min/+}$ but not Cnb1$^{\Delta IEC}$;*Apc*$^{Min/+}$ mice (Fig. 4c,d), which could be restored by transduction with Ad-*NFATC3*^{CA} (Fig. 2i, right and Supplementary Fig. 8g). Together, these data demonstrate that the microbiota and its Myd88-dependent recognition are sufficient for activation of calcineurin in CRC cells *in vitro* and are required for calcineurin-dependent tumor development *in vivo*.

Impaired barrier function in mice harboring intestinal tumors (Supplementary Fig. 9a)[5], perturbation of microbial stratification associated with intestinal tumors (Supplementary Fig. 9b and refs. [5,23–25]) and increased TLR expression by tumor cells (Supplementary Fig. 8a and ref. [36]) provide a mechanistic explanation for the pronounced activation of the calcineurin-NFAT pathway in tumors, as compared to that in healthy intestinal epithelium. Furthermore, differences in community structure (Fig. 4e) but not richness (Wilcoxon test $P = 0.27$ for Chao1 species-richness measure) of the transcriptionally active mucosa-adherent microbiota were observed between intestinal tumors and matched normal mucosa of *Apc*$^{Min/+}$ mice. Among the major species-level operational taxonomic units (OTUs) (average relative abundance >0.5%), six differed between the micro-biota associated with normal tissues and that associated with tumors from *Apc*$^{Min/+}$ mice (Fig. 4f). Notably, the OTUs that were increased in abundance in the tumor-associated microbiota belong to genera known to signal via TLR4 and Myd88—such as *Escherichia* and/or *Shigella*[37], as well as *Citrobacter*[38]. These alterations at the genus level also correspond to the increased abundance of Enterobacteriaceae and Proteobacteria at the family and phylum level, respectively (Fig. 4g). These data raise the possibility that, in addition to impaired bacterial stratification, specific alterations in bacterial communities may contribute to the TLR-dependent activation of calcineurin in intestinal tumors. This is further supported by findings obtained after antibiotic treatment (Supplementary Results and Supplementary Fig. 9c–f). Notably, the IEC-specific deletion of *Ppp3r1* did not affect the community structure of the commensal microbiota (Fig. 4e, Supplementary Results and Supplementary Fig. 10). As such, calcineurin does not regulate tumor development through effects on the composition of the commensal microbiota but rather through control of the epithelial response to tumor-associated changes in microbial stratification and composition. In addition, *Fusobacterium nucleatum* (a bacterium that promotes intestinal tumor development[25,29]) and endogenous damage-associated molecular pattern molecules (such as the TLR4 ligand high-mobility group box 1 (HMGB1) and the HMGB1-binding receptor for advanced glycation end products (RAGE)) did not contribute to calcineurin-dependent regulation of intestinal tumor development (Supplementary Results and Supplementary Fig. 11).

Calcineurin regulates tumor stem cell function

We next studied the molecular mechanisms of calcineurin- and NFAT-dependent tumor development. Because we did not observe any indirect effects of epithelial calcineurin on tumor-infiltrating cells (Supplementary Results and Supplementary Fig. 12a–c), we investigated whether calcineurin controls tumor development through direct, NFAT-dependent transcriptional regulation in tumor cells. Expression of candidate genes previously reported to be NFAT dependent—such as *Ptgs2* (ref. [10]), *Myc*[39], *Tp53* (ref. [40]), *Ccna2* (ref. [41]), *Mdm2* (ref. [42]), *Ddit4* (ref. [13]), *Pcna*[12] and *Cdkn1a*[12]—did not differ

between tumors from Cnb1$^{\Delta IEC}$;*Apc*$^{Min/+}$ mice and Cnb1^{WT};*Apc*$^{Min/+}$ mice (Supplementary Fig. 12d). Because tumors from Cnb1$^{\Delta IEC}$ and *Nfatc3*$^{\Delta IEC}$ mice exhibited reduced proliferation (Figs. 1f and 2h) and because tumor growth originates from proliferating intestinal stem cells[43], which also exhibit strong nuclear NFATc3 expression as revealed in mice expressing *EGFP* under the control of the leucine-rich repeat-containing G protein–coupled receptor 5 (*Lgr5*) promoter (*Lgr5-EGFP*-IRES-CreER^{T2} mice[43,44]) (Fig. 5a), we investigated the expression of stem cell–associated genes in tumors from Cnb1$^{\Delta IEC}$;*Apc*$^{Min/+}$ mice. Expression of *Lgr5*, olfactomedin 4 (*Olfm4*), doublecortin-like kinase 1 (*Dclk1*), tumor necrosis factor receptor superfamily, member 19 (*Tnfrsf19*) and the CRC-associated variant exon (v) 6 splice variant of CD44 antigen (*Cd44*v6; refs. [45,46]) were reduced in tumors from Cnb1$^{\Delta IEC}$;*Apc*$^{Min/+}$ mice (Fig. 5b,c), antibiotic-treated Cnb1^{WT};*Apc*$^{Min/+}$ but not Cnb1$^{\Delta IEC}$;*Apc*$^{Min/+}$ mice (Fig. 5b) and Ad-VIVIT–treated mice (as compared to Ad-*LacZ*–treated *Apc*$^{Min/+}$ mice) (Fig. 5d), and were partially reduced in tumors from *Nfatc3*$^{\Delta IEC}$;*Apc*$^{Min/+}$ mice (Supplementary Fig. 12e and data not shown (K.P.)). In accordance with the tumor-specific activation of calcineurin, normal Lgr5^{+} intestinal stem cells in *Apc*^{WT} mice showed predominantly cytoplasmic NFATc3 staining (Supplementary Fig. 12f), which is consistent with unimpaired *Lgr5*, *Olfm4* and *Dclk1* expression (Supplementary Fig. 12g) and with unaffected proliferation of normal IECs in Cnb1$^{\Delta IEC}$ mice (Supplementary Fig. 2c).

CD44 is a CRC stem cell marker, whose deletion in *Apc*$^{Min/+}$ mice leads to increased tumor apoptosis and reduced tumor multiplicity[46]. Similarly, CD44 splice forms containing variant exons, such as *Cd44*v6, identify human CRC stem cells[47], are of negative prognostic value in human CRC[45] and promote tumor development in the *Apc*$^{Min/+}$ model[48]. Consistent with the observation that apoptosis in *Cd44*-deficient *Apc*$^{Min/+}$ tumors predominantly affects the stem cell compartment[46], reduced numbers of eGFP^{+} tumor stem cells were detected in *Lgr5-EGFP*-IRES-CreER^{T2};Cnb1$^{\Delta IEC}$;*Apc*$^{Min/+}$ mice as compared to those in Cnb1^{WT} littermates (Fig. 5e). This reduction in the number of eGFP^{+} stem cells could be distinguished from a decrease in the mean eGFP expression per cell as a consequence of reduced NFAT-dependent activation of the *Lgr5* promoter (Fig. 5f; for NFAT-dependent *Lgr5* transcription see next paragraph). Furthermore, consistent with the observation of a reduction in the number of stem cells, tumors obtained from Cnb1$^{\Delta IEC}$;*Apc*$^{Min/+}$ mice gave rise to decreased numbers of organoids, as compared to those from Cnb1^{WT};*Apc*$^{Min/+}$ littermates (Fig. 5g).

The presence of NFAT-binding consensus sites in the promoters of *Cd44*, *Lgr5*, *Olfm4* and *Dclk1* (Supplementary Fig. 13a–d) and the recent description of NFATc1 binding to *Lgr5* and *Dclk1* in hair follicle stem cells[49] further raised the question of whether alterations in direct NFAT-dependent transcription contribute to the decreased expression of stem cell–associated genes in Cnb1$^{\Delta IEC}$;*Apc*$^{Min/+}$ tumors. Indeed, NFATc3 exhibited calcineurin-dependent binding to the promoters of *Cd44*, *Lgr5*, *Olfm4* and *Dclk1* in intestinal tumors *in vivo*, as determined by chromatin immunoprecipitation (ChIP)-qPCR analysis (Fig. 5h). Moreover, even in eGFP^{+} stem cells sorted from Cnb1$^{\Delta IEC}$;*Apc*$^{Min/+}$ tumors, thus avoiding indirect effects owing to a loss of stem cells, expression of *Cd44*v6, *Lgr5*, *Olfm4* and *Dclk1* were reduced as compared to stem cells obtained from Cnb1^{WT};*Apc*$^{Min/+}$ tumors (Fig. 5i). Also, shRNA-mediated knockdown of *PPP3R1*, and to a lesser degree of *NFATC3*, was

associated with decreased *LGR5* expression in SW707 human CRC cells (Supplementary Fig. 13e), whereas *CD44*, *OLFM4* and *DCLK1* were not expressed in this cell line. Together these data suggest that alterations in direct NFAT-dependent transcription, as well as a loss of tumor stem cells, contribute to decreased expression of stem cell–associated genes in $Cnb1^{\Delta IEC};Apc^{Min/+}$ tumors.

Cnb1-deficient $Apc^{Min/+}$ tumors and SW707 CRC cells showed reduced nuclear β-catenin expression and decreased T cell factor (TCF)- and lymphoid enhancer factor (LEF)-dependent transcription (Fig. 5j), respectively, suggesting positive regulation of Wnt signaling by epithelial calcineurin. Consistent with the observations that Lgr5 can promote canonical Wnt signaling through the binding of R-spondins[50] and that the expression of *Lgr5* was reduced in Cnb1-deficient $Apc^{Min/+}$ tumors (Fig. 5b) and SW707 CRC cells with stable knockdown of *PPP3R1* (Supplementary Fig. 13e), adenoviral-mediated expression of *Lgr5* in $Cnb1^{\Delta IEC};Apc^{Min/+}$ tumors (Supplementary Fig. 13f) partially restored nuclear β-catenin expression (Fig. 5j, left) and clonogenicity, as well as growth, in organoid cultures (Fig. 5j). In contrast, Ad-*LGR5* transduction had negligible effects on β-catenin expression (Fig. 5j, left) and on organoid growth and clonogenicity (Fig. 5j, right) in $Cnb1^{WT};Apc^{Min/+}$ mice. These results suggest that calcineurin-dependent regulation of Lgr5 expression supports tumor stem cell function and contributes, among other pathways, to calcineurin-dependent promotion of tumor development.

NFAT activation is associated with reduced CRC survival

Calcineurin expression and activity are increased in human CRC[51] and the growth of human CRC cells *in vitro* is dependent on calcineurin and NFATc3 (Fig. 3g). This suggests, similar to observations in mice, that calcineurin and NFAT regulate human CRC development. To further address this question, we investigated whether NFATc3 activation and nuclear translocation in human CRC are associated with cancer-related death in individuals with CRC. We stained for NFATc3 in CRC samples from 704 individuals for whom survival data was available for at least 5 years after diagnosis. In accordance with the observation of nuclear NFATc3 translocation in intestinal adenomas of $Apc^{Min/+}$ mice and thus at early stages of the adenoma-carcinoma sequence, nuclear NFATc3 expression was already observed at the T1 stage of CRC, with little or no correlation with the T ($r^2 = 0.004$, $P = 0.01$), N ($r^2 = 0.001$, $P = 0.2$) and M ($r^2 = 0.001$, $P = 0.3$) stages or with tumor grade ($r^2 = 0.00001$, $P = 0.9$). However, strong nuclear NFATc3 staining (staining score 2 or 3; $n = 593$ individuals) was associated with reduced survival (analysis limited to death from CRC), as compared to that in individuals with little or no nuclear NFATc3 staining (staining score 0 or 1; $n = 111$ individuals). These results demonstrate that the activation and nuclear translocation of NFATc3 is associated with increased death of individuals from CRC (Fig. 6a).

Recent exome and genome sequencing of samples from individuals with CRC revealed mutations in protein phosphatase 3 catalytic subunit beta (*PPP3CB*), which encodes the catalytic calcineurin subunit A (CnA)-β, that were associated with increased death of individuals from CRC[52,53] (http://www.cbioportal.org). Among these variants, $PPP3CB^{R410*}$ is a nonsense mutation–containing allele that is predicted to be associated

with loss of the autoinhibitory domain of CnA-β (ref. [54]). Consistently, ectopic expression of *PPP3CB*^{R410*} but not of *PPP3CB*^{WT} was associated with constitutive NFAT-dependent transcription in human SW707 CRC cells, which was also observed after shRNA-mediated silencing of *PPP3R1* (Fig. 6b). As such, human CRC is associated with increased calcineurin expression[51] and constitutively active CnA-β variants (Fig. 6b)[52,53], whereas activation of the calcineurin-NFAT pathway is associated with increased death of individuals from CRC (Fig. 6a).

DISCUSSION

Host immunity plays a critical role in the regulation of CRC. In addition to central functions of bone marrow–derived innate and adaptive immune cells, immune-associated signaling pathways in epithelial cells can promote intestinal tumor development[2–6]. Here we found that calcineurin and NFAT, two members of a pathway involved in immunity, are constitutively expressed by IECs and undergo selective activation in tumor tissue as a result of increased TLR expression by tumor cells, as well as altered stratification of the tumor-associated microbiota. After being activated by microbiota-derived TLR ligands, epithelial calcineurin supported the survival and proliferation of tumor stem cells and promoted tumor development in an NFAT-dependent manner (Fig. 6c).

These results support a role for microbial elements in the regulation of CRC[55,56] and provide novel insight into the molecular pathways linking tumor-associated changes in the microbiota to oncogenic epithelial signaling. Recent work documented alterations in the composition of the commensal microbiota associated with CRC development, which were characterized by an increase in the abundance of bacteria that are known to promote tumor growth[23,25,29,56,57]. Tumor-promoting alterations in microbial composition thereby act together with defects in epithelial barrier function[5] and microbial stratification[5,23–25] to enhance tumor growth in a manner dependent on signaling pathways in myeloid and epithelial cells[5,24,30,33]. Using *Apc*$^{Min/+}$ mice as a model of genetically driven intestinal tumor formation, we found bacterial translocation into intestinal adenomas, as well as an increase in the relative abundance of bacteria known to signal via TLR4 and Myd88. This suggests that defects in microbial stratification, as well as specific alterations in the composition of the commensal microbiota, contribute to the activation of oncogenic epithelial calcineurin. Notably, alterations in the tumor-associated microbiota were observed regardless of the IEC-specific deletion of calcineurin. This demonstrates that epithelial calcineurin does not regulate intestinal tumor development through effects on the composition of the commensal microbiota but rather through control of the epithelial response to changes in microbial composition and stratification along the adenoma-carcinoma sequence. In conclusion, these studies describe a novel epithelial pathway that integrates signals derived from the commensal microbiota to promote intestinal tumor development and that may be amenable to therapeutic targeting.

METHODS

Methods and any associated references are available in the online version of the paper.

ONLINE METHODS

Mice

Mice were handled, and all experiments were performed, in accordance with institutional guidelines and with the approval of the Ministerium für Energiewende, Landwirtschaft, Umwelt und ländliche Räume des Landes Schleswig-Holstein (Kiel, Germany) and the Harvard Medical Area Standing Committee on Animals (Boston, MA, USA). Mice were housed in a specific pathogen–free (SPF) barrier facility and were on C57BL/6J background, unless mentioned otherwise. GF C57BL/6J mice were housed at gnotobiotic facilities at the Max Planck Institute of Evolutionary Biology (Plön, Germany) and the Hannover Medical School (Hannover, Germany). Mice carrying *loxP*-flanked ('floxed') alleles of *Ppp3r1* (ref. [64]), *Nfatc1* (ref. [65]), and *Nfatc3* (ref. [66]) were previously described, and these were crossed with $Apc^{Min/+}$ mice[14] (Jackson Laboratory, Bar Harbor, Maine) and either villin-*Cre*[67] (Jackson Laboratory) or villin-$CreER^{T2}$ (ref. [68]) (gift of Dr. Sylvie Robine, Paris, France) mice as described. $Myd88^{-/-}$ mice[69] (gift of S. Akira, Osaka, Japan) were crossed with $Apc^{Min/+}$ mice as indicated. $Ager^{-/-}$;$Apc^{Min/+}$ mice (hereafter referred to as RAGE-KO mice) have been described before[70]. For Cnb1 deletion in adult mice, $Cnb1^{indΔIEC}$ mice received 1 mg of tamoxifen by intraperitoneal (i.p.) injection on five consecutive days at 12, 14, and 16 weeks of age, and the mice were sacrificed at 18 weeks of age. *Lgr5-EGFP*-IRES-$CreER^{T2}$ mice have been described before[44].

Animal studies were conducted in a gender- and age-matched manner using littermates for each experiment. Where indicated, mice were individually housed after weaning (3 weeks of age). Both male and female mice were used, and a formal process of randomization for treatment allocation was not performed. The number of animals used per group was based on previous experimental results and the observed variability. Macroscopic and microscopic tumor analysis was performed in a blinded manner (also see the section on 'Mouse tumor analysis and colitis studies'). For all other *in vitro* and *in vivo* analyses, investigators were not blinded to treatment allocation. Exclusion of animals from analyses by predefined criteria was not applied.

Mouse tumor analyses and colitis studies

Mice on the $Apc^{Min/+}$ background were sacrificed at week 6 for the analysis of microadenomas or at week 18 in all other experiments, unless mentioned otherwise. AOM-DSS studies were performed as described previously[3] with minor modifications. AOM (Sigma-Aldrich, Hamburg, Germany) was administered by i.p. injection at 12.5 mg per kg body weight (mg/kg). After 5 d, mice received 2.5% DSS (MP Biomedicals, Eschwege, Germany) in autoclaved water for 5 d followed by recovery on autoclaved water for 14 d. Three DSS cycles were performed. The disease activity index was determined as described before[71]. Histopathological scoring of tumors and inflammation[72] in H&E-stained sections was performed by a board-certified pathologist (C.R.), who was blinded to the genotype and experimental conditions of the samples.

Mouse antibiotic, adenoviral, antibody and inhibitor treatment

Antibiotic treatment of mice was performed by supplementation of drinking water with ampicillin (1 mg/ml), gentamicin (1 mg/ml), metronidazole (1 mg/ml), neomycin (1 mg/ml), and vancomycin (0.5 mg/ml) according to ref. [73]. For long-term antibiotic treatment, drinking water supplemented with antibiotics was continuously provided to mice from the age of 4 weeks until sacrifice at the age of 18 weeks.

Adenoviral (Ad5) constructs expressing constitutively active NFATc3 (Ad-*CMV-NFATC3*^{CA})[74], luciferase under control of a minimal promoter containing nine NFAT-binding sites (Ad-NFAT-*Luc*)[75], and LacZ (Ad5-*CMV-LacZ*; referred to as Ad-*LacZ*)[76] were obtained from Seven Hills Bioreagents (Cincinnati, OH, USA). Ad-*LGR5* was obtained from Vector Biolabs (Philadelphia, PA, USA). Ad5-*CMV*-VIVIT[77] was a gift from C.M. Norris (Lexington, KY, USA). Adenoviruses were prepared as described previously[78]. For adenovirus titering, the Adeno-X Rapid Titer Kit (Clontech, Saint-Germain-en-Laye, France) was used according to the manufacturer's instructions. For analysis of the restoration of tumor growth by Ad-*CMV-NFATC3*^{CA} or Ad-*LacZ*, mice received 3×10^9 adenoviruses by weekly i.p. injection from weeks 12 to 17. For analysis of the effects of Ad-VIVIT and Ad-*LacZ* on tumor multiplicity, tumor growth, tumor proliferation, tumor apoptosis, and RNA expression, mice received 3×10^9 adenoviruses by weekly i.p. injection from weeks 4 to 17. For analysis of tumor-associated luciferase expression, mice received 3×10^9 Ad-NFAT-*Luc* or Ad-*LacZ* viruses by i.p. injection for three consecutive days before tumor extraction. For restoration of LGR5 expression in intestinal tumors, mice received 3×10^9 Ad-*LacZ* or Ad-*LGR5* virus by i.p. injection daily for five consecutive days. Twenty-four hours after the final adenovirus administration, tumors were harvested for organoid generation.

Antibodies specific for mouse high-mobility group box 1 (HMGB1) protein (DPH1.1) or the HMGB1 domain BoxA were obtained from HMGBiotech (Milan, Italy). For *in vivo* blocking, mice received 200 μg anti-HMGB1 or isotype control by i.p. injection, or 400 μg recombinant BoxA protein or vehicle control by i.p. injection. Tumors were analyzed 8 h after injection.

Fecal microbial transfer

For microbial reconstitution of GF mice, 6-week-old WT C57BL/6J mice received fecal material obtained from individually housed Cnb1$^{\Delta IEC}$;*Apc*$^{Min/+}$ or Cnb1^{WT};*Apc*$^{Min/+}$ mice. Stool pellets were freshly dissolved in PBS with 0.05% l-cysteine hydrochloride (Sigma-Aldrich; 4 pellets per 5 ml of PBS) and mice received 100 μl of solution by gavage. After 3 weeks, mice were investigated in the AOM-DSS protocol as outlined in the section 'Mouse tumor analyses and colitis studies'. For microbial reconstitution of *Apc*$^{Min/+}$ mice, 4-week-old mice were treated with antibiotics (see 'Mouse antibiotic, adenoviral, antibody and inhibitor treatment') for 3 weeks, followed by gavage of fecal microbiota as described above. Mice were sacrificed at 18 weeks of age for tumor analyses.

Mouse intestinal organoids, adenovirus treatment and TLR blocking

Intestinal organoids were obtained as described previously[79] with minor modifications. Briefly, tumors were separated from surrounding normal tissue, washed in PBS ten times, incubated in 2 mM EDTA (Life Technologies) in PBS for 30 min, passed through a 70-μm cell strainer, and seeded into Matrigel (BD Biosciences, Heidelberg, Germany) with growth medium containing advanced Dulbecco's modified Eagle's medium–nutrient mixture F12 (DMEM/F12; Life technologies), 1× Glutamax (Life technologies), 1M HEPES (Life Technologies), penicillin-streptomycin (Biochrom, Berlin, Germany), 1× N2 supplement (Life Technologies), 1× B27 supplement (Life Technologies), 1.25 mM *N*-acetylcysteine (Sigma-Aldrich), 50 ng/μl epidermal growth factor (EGF; Life Technologies) and 20% conditioned supernatant containing noggin. For organoid preparation from Apc^{WT} tissue, 20% conditioned supernatant containing R-spondin was further added. For adenovirus treatment, crypt cells were incubated at 37 °C with Ad-*LacZ*, Ad-VIVIT or Ad-*CMV-NFATC3*^{CA} for 6 h at a multiplicity of infection of 100 before seeding into Matrigel. For blocking of HMGB1 and TLR4, organoids were treated with 10 μg/ml anti-HMGB1 antibody (DPH1.1), 10 μg/ml anti–mouse TLR4 (MTS510, BioLegend) antibody or isotype control antibody, or 10 μg/ml BoxA or vehicle control for 7 d, with a change of medium every 2 d.

Cell culture, lentiviral shRNA transduction and human CnA variants

HT-29, Caco-2, HCT-15, HCT-115, HCT-116, SW707, SW480, LoVo, Colo 320, and Jurkat cells were cultured in RPMI-1640 medium with 10% fetal bovine serum (FBS). MODE-K and CMT-93 cells were cultured in DMEM with 10% FBS. All cell lines were obtained from the American Type Culture Collection (ATCC) (LGC Standards GmbH, Wesel, Germany), unless otherwise mentioned. YAMC, IMCE, and IMCE-*Ras* cell lines (see ref. [80]) were generated and generously provided by Dr. Robert H. Whitehead (Nashville, TN, USA) and were cultured as previously described[80]. MODE-K cells were generated and generously provided by Dominique Kaiserlian (Lyon, France)[81]. None of the cell lines mentioned above belong to those commonly misidentified (International Cell Line Authentication Committee (ICLAC); http://iclac.org/databases/cross-contaminations/). Authentication of commercially available cell lines was performed by the ATCC. Cell lines not commercially available were obtained from the primary investigators who generated the respective cell lines and were thus not authenticated further. For serum starvation, cells were washed twice with PBS and incubated with growth medium (see above), with or without FBS for 2 h before cell harvesting, and luciferase analysis was performed as described below. For analysis of cell growth, 5×10^3 cells were seeded in 24-well plates (Greiner Bio One, Frickenhausen, Germany), and cells were counted every 2 d. All cell lines repeatedly tested negative for mycoplasma contamination in routine screenings.

SW707 cells were transduced with lentiviruses expressing an shRNA directed against human *PPP3R1* (TRCN0000002758), *NFATC3* (TRCN0000014532) or a nontargeting control (nonmammalian shRNA control) (all from Sigma-Aldrich) at a multiplicity of infection of 5 in the presence of polybrene (8 μg/μl). Stably transduced cells were cloned using cloning cylinders, and clones were selected based on target gene knockdown as determined by quantitative PCR and reduced expression of an NFAT-dependent luciferase construct.

The open reading frame of human CnA (*PPP3CB*), with or without *PPP3CB* variants identified in CRC[52,53] (http://www.cbioportal.org), was synthesized (GeneCust, Luxembourg) and subcloned into pcDNA3.1.

Calcium-flux measurements

Calcium-flux measurements were performed using a FlexStation 3 microplate reader (Molecular Devices, Biberach, Germany) 24 h after cells were plated in a 96-well flat-bottom plate. Calcium-loading dye (FLIPR Calcium 5 Assay Kit, Molecular Devices) was added according to the manufacturer's instructions with 1 h of incubation at 37 °C. Cells were then stimulated with Pam3CSK4 (10 μg/ml), LPS (1 μg/ml) or PMA (50 ng/ml) and ionomycin (1 mM).

Western blotting, nuclear extracts and electrophoretic mobility shift assays (EMSAs)

Western blotting, nuclear extracts, and EMSAs were performed as described previously[82]. For EMSAs, probes were used that contain an NFAT–AP-1 consensus site (5′-CAAAAGGCGGAAAGAAACAGTCATTTC-3′) or an NF-κB consensus site (5′-AGTTGAGGGGACTTTCCCAGGC-3′). For EMSA and western blotting, cells were stimulated for 4 h with 1 μg/ml LPS (Sigma-Aldrich), 10 μg/ml Pam3CSK4 (InvivoGen, Toulouse, France), 100 μg/ml pIpC (InvivoGen), 10 μg/ml flagellin (InvivoGen), 100 μg/ml *E. coli* DNA (InvivoGen) or 50 ng/ml PMA (Sigma-Aldrich) and 1 mM ionomycin (Sigma-Aldrich). Where indicated, cells were incubated for 2 h with 2 mM EGTA (Life Technologies), 5 μM BTP2 (Merck Millipore, Darmstadt, Germany) or 10 μM U73122 (Sigma-Aldrich). For ERK1-ERK2 activation, the indicated cell lines were serum-starved for 2 h and treated with EGF or vascular endothelial growth factor (VEGF) at 10 ng/ml (PeproTech, Hamburg, Germany) for the indicated periods. Where indicated, YAMC, IMCE and IMCE-*Ras* cells were incubated at 33 °C with Ad-*LacZ*, Ad-VIVIT or Ad-Cn^{CA} (which expresses truncated and constitutively active CnA-β) at a multiplicity of infection of 50 before further treatment or analysis. For western blotting, the following antibodies were used: anti–human and mouse NFATc1 (7A6, 1:200, Santa Cruz, Heidelberg, Germany), anti–human and mouse NFATc2 (4G6G5, 1:200, Santa Cruz), anti–human and mouse NFATc3 (M75 or F1, 1:200, Santa Cruz), anti–human and mouse NFATc4 (H74, 1:200, Santa Cruz), anti–human and mouse ERK1-ERK2 (137F5, 1:1,000, Cell Signaling Technology, Leiden, the Netherlands), anti–human and mouse phospho–ERK1-ERK2 (D13.14.4E, 1:1,000, Cell Signaling Technology), anti–human and mouse β-actin (A2066, 1:2,000, Sigma-Aldrich), anti–human and mouse Cnb1 (C0581, 1:3,000, Sigma-Aldrich), anti–human and mouse STAT3 (79D7, 1:1,000, Cell Signaling Technology), anti–human and mouse phospho-STAT3 (Y705, 1:1,000 Cell Signaling Technology), and anti–human and mouse Sp1 (ABE135, 1:1,000, Merck Millipore).

Luciferase assays

For luciferase assays in cultured cell lines, plasmids expressing firefly luciferase under control of a minimal NFAT-dependent promoter[83] (11783, Addgene, Cambridge, MA, USA), a TCF-LEF–dependent promoter[84] (TOPFlash, 12456, Addgene) or a NF-κB–dependent promoter (Promega, Mannheim, Germany) were transfected, along with a plasmid expressing *Renilla* luciferase (phRluc, Promega) for normalization of transfection

efficacy, into cells. Where indicated, WT or mutated *PPP3CB* or an empty pcDNA3.1 was transfected along with the plasmids described above. 24 h after transfection with Lipofectamine 2000 (Life Technologies), according to the manufacturer's instructions, cells were stimulated using 1 μg/ml LPS (Sigma-Aldrich), 10 μg/ml Pam3CSK4 (InvivoGen), 100 μg/ml pIpC (InvivoGen), 10 μg/ml flagellin (InvivoGen), 100 μg/ml *E. coli* DNA (InvivoGen), 10 μg/ml cyclosporine A (Sigma-Aldrich), 400 ng/ml recombinant Wnt3a (R&D Systems, Minneapolis, MN, USA) or 50 ng/ml PMA (Sigma-Aldrich) and 1 μM ionomycin (Sigma-Aldrich). 16 h after stimulation, luciferase expression was analyzed with the Dual-Glo-Luciferase Assay System (Promega) according to the manufacturer's instructions using a FlexStation 3 (Molecular Devices).

For luciferase analysis in tumor tissues, mice were injected daily for three consecutive days with 3×10^9 adenoviruses expressing NFAT-dependent firefly luciferase (Ad-NFAT-*Luc*[75], Seven Hills Bioreagents, Cincinnati, OH, USA) or Ad-*LacZ* in 100 μl PBS by i.p. injection. 24 h after the last injection, tumors were extracted, washed in PBS and lyzed in passive lysis buffer (Promega). Protein concentration was determined, using protein assay dye reagent (Bio-Rad Laboratories, Hercules, CA, USA) according to the manufacturer's instructions, and used for normalization of luciferase activity.

Immunohistochemistry (IHC), immunofluorescence and tissue microarrays (TMAs)

Immunohistochemistry and immunofluorescence stainings were performed using paraffin-embedded tissues. Antigen retrieval was performed in citrate buffer (1.8% 0.1 M citric acid, 8.2% 0.1 M sodium citrate) for 25 min at 95 °C; sections were washed in PBS, incubated for 10 min in H_2O_2 (for IHC), blocked in 1% BSA in PBS–Tween 20, incubated for 1 h at room temperature in primary antibody, and washed in PBS. For immunohistochemistry, sections were incubated in EnVision secondary antibody (Dako, Hamburg, Germany) for 30 min at room temperature (RT), washed, counterstained with hemalaun and embedded using Entellan (Merck Millipore). For immunofluorescence, sections were incubated with Alexa Fluor 488–or Alexa Fluor 594–conjugated secondary antibodies (Life Technologies) and DAPI (1 μg/ml, Sigma-Aldrich) for 1 h at RT, washed, and embedded using FluorSave (Merck Millipore). For immunohistochemistry, the following antibodies were used: anti–mouse Cnb1 (C-0581, 1:500, Sigma-Aldrich), anti–human and mouse NFATc1 (7A6, 1:100, Santa Cruz), anti–human and mouse NFATc2 (HPA024369, 1:60, Sigma-Aldrich), anti–human and mouse NFATc3 (HPA023844, 1:60, Sigma-Aldrich), anti–human and mouse NFATc4 (HPA031641, 1:60, Sigma-Aldrich), anti–human and mouse NF-κB (C22B4, 1:50, Cell Signaling Technology), anti–human and mouse phospho–NF-κB (S276, 1:50, Cell Signaling Technology), anti–human and mouse STAT3 (79D7, 1:50, Cell Signaling Technology), anti–human and mouse phospho-STAT3 (Y705, 1:100, Cell Signaling Technology), anti–human and mouse DCLK1 (ab31704, 1:1,000, Abcam, Cambridge, UK), anti–human and mouse β-catenin (9587, 1:1,000, Cell Signaling Technology), and Envision anti–rabbit IgG and anti–mouse IgG (Dako). For immunofluorescence, the following antibodies were used: anti–human and mouse NFATc3 (F1, 1:50, Santa Cruz), anti–human and mouse NFATc3 (HPA023844, 1:60, Sigma-Aldrich), anti–human and mouse Ki-67 (D3B5, 1:400, Cell Signaling Technology), anti–human and mouse cleaved caspase-3 (D175, 1:300, Cell Signaling Technology), anti–lysozyme C (C-19, 1:50, Santa Cruz), anti-

GFP (D5.1, 1:75, Cell Signaling Technology) and anti-FLAG (M2, 1:10,000, Sigma-Aldrich). Images were taken using a Zeiss Axioplan 2 (Carl Zeiss, Jena, Germany).

Tissue microarrays included matched normal mucosa and CRC samples from 704 individuals with CRC for whom survival data was available for at least 5 years following diagnosis. Studies were approved by the ethics committee of the University Medical Center Schleswig-Holstein, Kiel, Germany, and all subjects provided written informed consent. Survival analysis is based on centralized recordings by the State of Schleswig-Holstein (Krebsregister Schleswig-Holstein), which also records the cause of death. Individuals with non-CRC–related death during follow-up were excluded from this study. NFATc3 staining was performed in a standardized manner for all TMAs using the same protocol and a similar antibody lot: antigen retrieval was performed using 10 mM citrate buffer (pH 6.0) and a DakoCytomation Pascal pressure chamber (DakoCytomation, Hamburg, Germany) at 125 °C for 1 min. After a blocking step with Hydrogen Peroxide Block (Thermo Scientific) and Ultra V Block (Thermo Scientific), samples were incubated with anti–human and mouse NFATc3 (HPA023844, 1:60, Sigma-Aldrich) at 4 °C overnight followed by detection using Histofine simple stain MAX PO Multi detection reagent (Nichirei Biosciences Inc., Tokyo, Japan) in combination with the DAB Peroxidase Substrate Kit (Vector Laboratories Inc., Burlingame, USA). Counterstaining was done with haematoxylin (Dr. K. Hollborn & Söhne GmbH & Co KG, Leipzig, Germany). Cytoplasmic and nuclear staining intensities of NFATc3 were separately scored on a scale from 0 to 3 in a blinded manner, and the following categories were assigned (for examples of staining intensity, please refer to Fig. 6a): 0, no expression; 1, weak expression; 2, moderate expression; 3, strong expression.

For analysis of barrier dysfunction, mice were orally administered 0.6 mg per g body weight of FITC-dextran (4 kDa, Sigma-Aldrich) in 100 μl PBS, and blood was collected after 4 h. Relative fluorescence units were measured in serum using a FlexStation 3 microplate reader (Molecular Devices). For staining, small intestines were embedded in Tissue-Tek O.C.T. compound (Sakura, Alphen aan den Rijn, the Netherlands), and sections were prepared using a Leica CM1850 (Leica Biosystems, Wetzlar, Germany). Sections were directly incubated with DAPI (1 μg/ml, Sigma-Aldrich) for 10 min at room temperature, washed, and embedded using FluorSave (Merck Millipore).

For senescence-associated staining, the Senescence β-galactosidase Staining Kit (Cell Signaling) was used according to the manufacturer's instructions. Sections of unfixed small intestines, embedded in Tissue-Tek O.C.T. compound, were used.

Live-cell imaging

For live-cell imaging, SW707 human CRC cells were transfected, using Lipofectamine 2000 according to the manufacturer's instructions (Life Technologies), with a construct expressing an NFATc3-GFP fusion protein[15] (21664, Addgene). 24 h after transfection, cells were stimulated with 1 μM LPS, and images were acquired using an FV1000 confocal laser-scanning microscope (Olympus, Hamburg, Germany) equipped with a U Plan S Apo 60× oil-immersion objective (numerical aperture (N.A.) 1.40) and Olympus Fluoview Software (3.0a).

Fluorescence *in situ* hybridization

For fluorescence *in situ* hybridization, tissues were incubated in Carnoy's fixative (46% ethanol, 46% glacial acetic acid, 8% chloroform) overnight and embedded in paraffin. Slides were incubated at 50 °C for 1 h with hybridization buffer (18% 5 M NaCl, 2% 1 M Tris-HCl pH 7.4, 0.5% SDS) and 25 ng of Cy3-labeled universal bacterial probe (Bact338, see Supplementary Table 1 for nucleotide sequence; Eurofins, Ebersberg Germany), washed for 5 min in washing buffer (900 mM NaCl, 2% 1 M Tris-HCl pH 7.4, 0.06% SDS), and incubated with DAPI (1 μg/ml, Sigma-Aldrich) for 5 min.

Flow cytometry and flow sorting

Flow cytometry was performed as described previously[85]. Briefly, tumors were excised, washed in PBS and incubated in Hank's balanced salt solution (HBSS, Biochrom) with 1 mg/ml collagenase D (Biochrom), 20 ng/ml DNase (Roche, Mannheim, Germany) and 50 μg/ml dispase II (Roche) for 30 min at 37 °C. Cells were passed through a 70-μm cell strainer (BD Biosciences), washed in PBS and incubated in FcR blocking reagent (Miltenyi Biotec, Bergisch Gladbach, Germany) in 0.5% BSA (SERVA Electrophoresis, Heidelberg, Germany) and 2 mM EDTA (Life Technologies) in PBS for 10 min at 4 °C. Fixable viability dye eFluor 450 (eBiosciences, Frankfurt, Germany) was added to all stainings for exclusion of dead cells, and cells were stained with monoclonal antibodies for 20 min at 4 °C. All antibodies were purchased from BioLegend (Fell, Germany), except for anti-CD8 (BD Biosciences). For the detection of iNKT cells, staining with PBS57-loaded CD1d tetramers (60 min, 4 °C, NIH Tetramer Core Facility, Atlanta, USA) was performed. Data were collected using a BD Biosciences FACSVerse and were analyzed using FlowJo (Tree Star Inc., Ashland, OR).

For sorting of $eGFP^+$ stem cells, cells were extracted as mentioned above. After passage through a 70-μm cell strainer, cells were incubated in 3 ml TrypLE (Life Technologies) including 2,000 U/ml DNase (Sigma-Aldrich) for 30 min at 37 °C, passed through a 40-μm cell strainer and then sorted using a BD FACSAria (BD Biosciences).

RNA extraction and quantitative PCR

RNA of tissue was extracted using the RNeasy Mini Kit (Qiagen, Hilden, Germany). 2 μg RNA were transcribed into cDNA using the High-Capacity cDNA Reverse-Transcription Kit (Life Technologies) and quantitative PCR was performed as described previously[78]. PCR primers are listed in Supplementary Table 1.

RNA from the sorted cells was extracted using the Arturus PicoPure RNA Isolation Kit (Life Technologies) according to the manufacturer's instructions.

Chromatin immunoprecipitation (ChIP)

Tissue was cross-linked in 1.5% formaldehyde, and chromatin was purified using the SimpleChIP Plus Enzymatic Chromatin IP Kit (Cell Signaling Technology) according to the manufacturer's instructions. 10 μg of digested chromatin was incubated overnight at 4 °C with 5 μg anti–human and mouse NFATc3 antibody (M75, Santa Cruz) or isotype and were subsequently immunoprecipitated with Protein G magnetic beads. DNA was purified and

analyzed by qPCR. Input chromatin without immunoprecipitation was used for normalization in qPCR. PCR primers are listed in Supplementary Table 1.

16S rRNA sequencing and analysis

Transcriptionally active[86] members of the mucosa-attached microbiota were analyzed by performing 16S rRNA amplicon sequencing using bacterial cDNA as template for PCR. RNA was extracted using the AllPrep DNA/RNA Mini Kit (Qiagen). Amplification of the V1-V2 region of the 16S rRNA gene was performed using the primer pair 27F and 338R with flanking multiplex identifier (MID)-adaptors[87]. Amplicons were sequenced on the Illumina MiSeq platform using the MiSeq V3 sequencing kit to produce 300-bp pair-end reads. Fastq sequences were merged using FLASH software[88], and merged reads were then filtered based on quality (>90% of nucleotides must have quality score 30 or higher for every read). Chimeras were removed using Uchime v6.0.307 (ref. [89]), and each sample was then subsequently normalized to 20,000 random reads per sample. Sequences were classified with RDP classifier[90], and species-level OTUs were clustered *de novo* using Usearch v6.0.307 (ref. [91]). All taxonomy tables were created using Perl scripts for the follow-up analysis. Statistical analysis of alpha-diversity and beta-diversity was carried out using the Vegan[92] package in R.

Statistical analysis

For data sets of unknown or skewed distribution, nonparametric statistical analysis was performed using the Mann-Whitney *U* test or, in case of multiple testing, the Kruskal-Wallis test followed by the Dunn's test for multiple comparisons, and individual samples, as well as the median, were plotted. In the case of Gaussian distribution, parametric statistical analysis was performed using the two-tailed Student's *t*-test or, in case of multiple testing, one-way ANOVA, and the mean ± s.e.m. were plotted. For the disease activity index (DAI) analysis, the Wilcoxon matched-pairs signed-rank test was applied. For survival analysis, the log-rank test was applied. For evaluation of colocalization of DAPI and NFATc3, the Pearson correlation coefficient was used. Measures of location and variability, as well as the statistical test applied, are indicated for each data set.

Supplementary Material

Refer to Web version on PubMed Central for supplementary material.

Acknowledgments

The authors thank L.H. Glimcher (Weill Cornell Medical College), M.B. Greenblatt (Weill Cornell Medical College) and A.O. Aliprantis (Brigham and Women's Hospital, Harvard Medical School) for *Nfatc1*$^{fl/fl}$ mice and for helpful discussions; G.R. Crabtree (Center for Regenerative Therapies, Dresden) for *Ppp3r1*$^{fl/fl}$ and *Nfatc3*$^{fl/fl}$ mice; L. Niederreiter (Addenbrooke Hospital) for help with *in situ* hybridization; K. Schmidt, A. Gerneth, M. Pein (University Medical Center Schleswig-Holstein), S. Krüger (University Medical Center Schleswig-Holstein) and M. Jäger (Stanford University) for assistance with immunofluorescence, immunohistochemistry and TMA stainings; K. Cloppenborg-Schmidt (Institute for Experimental Medicine) for assistance with NGS library preparation; S. Robine (Institut Curie CNRS) for villin-CreER^{T2} mice; S. Akira (Research Institute for Microbial Diseases) for *Myd88*$^{-/-}$ mice; R.H. Whitehead (Vanderbilt University Medical Center) for the YAMC, IMCE and IMCE-*Ras* cells; C.M. Norris (Molecular and Biomedical Pharmacology) for the Ad5-*CMV*-VIVIT construct; R. Moon (University of Washington) for the TOPFlash plasmid; A. Rao (La Jolla Institute for Allergy and Immunology) for the NFAT-*Luc* and *NFATc3-eGFP* plasmids; and W. Garrett (Harvard T.H. Chan School of Public Health), S. Schölch and D.E. Stange (University Medical Center Dresden) for helpful discussions. This work was supported by the Deutsche

Forschungsgemeinschaft (DFG) grants ZE814/5-1 (S.Z.), BA2863/5-1 (J.F.B.) and CH279/5-1 (T.C.), the European Research Council (ERC) starting grant 336528 (S.Z.), a Postdoctoral Fellowship Award from the Crohn's and Colitis Foundation of America (S.Z.), the European Commission (Marie Curie International Reintegration grant 256363; S.Z.), the DFG Excellence Cluster 'Inflammation at Interfaces' (S.Z. and J.F.B.), the DFG Excellence Cluster 'Center for Regenerative Therapies' (S.Z.); the US National Institutes of Health grants DK044319 (R.S.B.), DK051362 (R.S.B.), DK053056 (R.S.B.) and DK088199 (R.S.B.), the Harvard Digestive Diseases Center (HDDC) grant DK0034854 (R.S.B.), and the AIRC grant IG-14233 (M.E.B.).

References

1. Terzić J, Grivennikov S, Karin E, Karin M. Inflammation and colon cancer. Gastroenterology. 2010; 138:2101–2114. [PubMed: 20420949]
2. Bollrath J, et al. gp130-mediated Stat3 activation in enterocytes regulates cell survival and cell cycle progression during colitis-associated tumorigenesis. Cancer Cell. 2009; 15:91–102. [PubMed: 19185844]
3. Greten FR, et al. IKKβ links inflammation and tumorigenesis in a mouse model of colitis-associated cancer. Cell. 2004; 118:285–296. [PubMed: 15294155]
4. Grivennikov S, et al. IL-6 and Stat3 are required for survival of intestinal epithelial cells and development of colitis-associated cancer. Cancer Cell. 2009; 15:103–113. [PubMed: 19185845]
5. Grivennikov SI, et al. Adenoma-linked barrier defects and microbial products drive IL-23– and IL-17–mediated tumor growth. Nature. 2012; 491:254–258. [PubMed: 23034650]
6. Schwitalla S, et al. Intestinal tumorigenesis initiated by dedifferentiation and acquisition of stem cell–like properties. Cell. 2013; 152:25–38. [PubMed: 23273993]
7. Li H, Rao A, Hogan PG. Interaction of calcineurin with substrates and targeting proteins. Trends Cell Biol. 2011; 21:91–103. [PubMed: 21115349]
8. Adami J, et al. Cancer risk following organ transplantation: a nationwide cohort study in Sweden. Br J Cancer. 2003; 89:1221–1227. [PubMed: 14520450]
9. Dantal J, et al. Effect of long-term immunosuppression in kidney graft recipients on cancer incidence: randomized comparison of two cyclosporin regimens. Lancet. 1998; 351:623–628. [PubMed: 9500317]
10. Duque J, Fresno M, Iñiguez MA. Expression and function of the nuclear factor of activated T cells in colon carcinoma cells: involvement in the regulation of cyclooxygenase-2. J Biol Chem. 2005; 280:8686–8693. [PubMed: 15632146]
11. Jauliac S, et al. The role of NFAT transcription factors in integrin-mediated carcinoma invasion. Nat Cell Biol. 2002; 4:540–544. [PubMed: 12080349]
12. Masuo T, Okamura S, Zhang Y, Mori M. Cyclosporine A inhibits colorectal cancer proliferation probably by regulating expression levels of c-Myc, $p21^{WAF1/CIP1}$ and proliferating cell nuclear antigen. Cancer Lett. 2009; 285:66–72. [PubMed: 19481339]
13. Zhou Y, Wang Q, Guo Z, Weiss HL, Evers BM. Nuclear factor of activated T cell–c3 inhibition of mammalian target of rapamycin signaling through induction of regulated in development and DNA damage response 1 in human intestinal cells. Mol Biol Cell. 2012; 23:2963–2972. [PubMed: 22696685]
14. Moser AR, Pitot HC, Dove WF. A dominant mutation that predisposes to multiple intestinal neoplasia in the mouse. Science. 1990; 247:322–324. [PubMed: 2296722]
15. Aramburu J, et al. Affinity-driven peptide selection of an NFAT inhibitor more selective than cyclosporin A. Science. 1999; 285:2129–2133. [PubMed: 10497131]
16. Rivera A, Maxwell SA. The p53-induced gene–6 (proline oxidase) mediates apoptosis through a calcineurin-dependent pathway. J Biol Chem. 2005; 280:29346–29354. [PubMed: 15914462]
17. Shinmen N, et al. Activation of NFAT signal by p53K120R mutant. FEBS Lett. 2009; 583:1916–1922. [PubMed: 19416725]
18. Woodrow M, Clipstone NA, Cantrell D. p21ras and calcineurin synergize to regulate the nuclear factor of activated T cells. J Exp Med. 1993; 178:1517–1522. [PubMed: 8228805]
19. Armesilla AL, et al. Vascular endothelial growth factor activates nuclear factor of activated T cells in human endothelial cells: a role for tissue factor gene expression. Mol Cell Biol. 1999; 19:2032–2043. [PubMed: 10022890]

20. Köenig A, et al. NFAT-induced histone acetylation relay switch promotes c-Myc–dependent growth in pancreatic cancer cells. Gastroenterology. 2010; 138:1189–1199. [PubMed: 19900447]
21. Saneyoshi T, Kume S, Amasaki Y, Mikoshiba K. The Wnt-calcium pathway activates NFAT and promotes ventral cell fate in *Xenopus* embryos. Nature. 2002; 417:295–299. [PubMed: 12015605]
22. Wang JY, et al. Involvement of store-operated calcium signaling in EGF-mediated *COX-2* gene activation in cancer cells. Cell Signal. 2012; 24:162–169. [PubMed: 21924350]
23. Castellarin M, et al. Fusobacterium nucleatum infection is prevalent in human colorectal carcinoma. Genome Res. 2012; 22:299–306. [PubMed: 22009989]
24. Dejea CM, et al. Microbiota organization is a distinct feature of proximal colorectal cancers. Proc Natl Acad Sci USA. 2014; 111:18321–18326. [PubMed: 25489084]
25. Kostic AD, et al. Genomic analysis identifies association of *Fusobacterium* with colorectal carcinoma. Genome Res. 2012; 22:292–298. [PubMed: 22009990]
26. Wang EL, et al. High expression of toll-like receptor 4 and myeloid differentiation factor 88 signals correlates with poor prognosis in colorectal cancer. Br J Cancer. 2010; 102:908–915. [PubMed: 20145615]
27. Arthur JC, et al. Intestinal inflammation targets cancer-inducing activity of the microbiota. Science. 2012; 338:120–123. [PubMed: 22903521]
28. Dove WF, et al. Intestinal neoplasia in the Apc^{Min} mouse: independence from the microbial and natural killer (beige locus) status. Cancer Res. 1997; 57:812–814. [PubMed: 9041176]
29. Kostic AD, et al. Fusobacterium nucleatum potentiates intestinal tumorigenesis and modulates the tumor-immune microenvironment. Cell Host Microbe. 2013; 14:207–215. [PubMed: 23954159]
30. Lee SH, et al. ERK activation drives intestinal tumorigenesis in $Apc^{Min/+}$ mice. Nat Med. 2010; 16:665–670. [PubMed: 20473309]
31. Li Y, et al. Gut microbiota accelerate tumor growth via c-jun and STAT3 phosphorylation in $Apc^{Min/+}$ mice. Carcinogenesis. 2012; 33:1231–1238. [PubMed: 22461519]
32. Rakoff-Nahoum S, Medzhitov R. Regulation of spontaneous intestinal tumorigenesis through the adaptor protein MyD88. Science. 2007; 317:124–127. [PubMed: 17615359]
33. Scheeren FA, et al. A cell-intrinsic role for TLR2-MYD88 in intestinal and breast epithelia and oncogenesis. Nat Cell Biol. 2014; 16:1238–1248. [PubMed: 25362351]
34. Song X, et al. Alterations in the microbiota drive interleukin-17C production from intestinal epithelial cells to promote tumorigenesis. Immunity. 2014; 40:140–152. [PubMed: 24412611]
35. Zanoni I, et al. CD14 regulates the dendritic cell life cycle after LPS exposure through NFAT activation. Nature. 2009; 460:264–268. [PubMed: 19525933]
36. Santaolalla R, et al. TLR4 activates the β-catenin pathway to cause intestinal neoplasia. PLoS One. 2013; 8:e63298. [PubMed: 23691015]
37. Rallabhandi P, et al. Differential activation of human TLR4 by *Escherichia coli* and *Shigella flexneri* 2a lipopolysaccharide: combined effects of lipid A acylation state and *TLR4* polymorphisms on signaling. J Immunol. 2008; 180:1139–1147. [PubMed: 18178854]
38. Liu S, Kielian T. Microglial activation by *Citrobacter koseri* is mediated by TLR4- and MyD88-dependent pathways. J Immunol. 2009; 183:5537–5547. [PubMed: 19812209]
39. Buchholz M, et al. Overexpression of c-myc in pancreatic cancer caused by ectopic activation of NFATc1 and the Ca^{2+}-calcineurin signaling pathway. EMBO J. 2006; 25:3714–3724. [PubMed: 16874304]
40. Wu X, et al. Opposing roles for calcineurin and ATF3 in squamous skin cancer. Nature. 2010; 465:368–372. [PubMed: 20485437]
41. Carvalho LD, et al. The NFAT1 transcription factor is a repressor of cyclin A2 gene expression. Cell Cycle. 2007; 6:1789–1795. [PubMed: 17637565]
42. Zhang X, et al. Transcription factor NFAT1 activates the *Mdm2* oncogene independent of p53. J Biol Chem. 2012; 287:30468–30476. [PubMed: 22787160]
43. Barker N, et al. Crypt stem cells as the cells-of-origin of intestinal cancer. Nature. 2009; 457:608–611. [PubMed: 19092804]
44. Barker N, et al. Identification of stem cells in small intestine and colon by marker gene *Lgr5*. Nature. 2007; 449:1003–1007. [PubMed: 17934449]

45. Mulder JW, et al. Colorectal cancer prognosis and expression of exon v6–containing CD44 proteins. Lancet. 1994; 344:1470–1472. [PubMed: 7526103]
46. Zeilstra J, et al. Deletion of the WNT target and cancer stem cell marker CD44 in *Apc*$^{Min/+}$ mice attenuates intestinal tumorigenesis. Cancer Res. 2008; 68:3655–3661. [PubMed: 18483247]
47. Todaro M, et al. CD44v6 is a marker of constitutive and reprogrammed cancer stem cells driving colon cancer metastasis. Cell Stem Cell. 2014; 14:342–356. [PubMed: 24607406]
48. Zeilstra J, et al. Stem cell CD44v isoforms promote intestinal cancer formation in *Apc*^{min} mice downstream of Wnt signaling. Oncogene. 2014; 33:665–670. [PubMed: 23318432]
49. Keyes BE, et al. Nfatc1 orchestrates aging in hair follicle stem cells. Proc Natl Acad Sci USA. 2013; 110:E4950–E4959. [PubMed: 24282298]
50. de Lau W, et al. Lgr5 homologs associate with Wnt receptors and mediate R-spondin signaling. Nature. 2011; 476:293–297. [PubMed: 21727895]
51. Lakshmikuttyamma A, Selvakumar P, Kanthan R, Kanthan SC, Sharma RK. Increased expression of calcineurin in human colorectal adenocarcinomas. J Cell Biochem. 2005; 95:731–739. [PubMed: 15832371]
52. Cancer Genome Atlas Network. Comprehensive molecular characterization of human colon and rectal cancer. Nature. 2012; 487:33–337.
53. Seshagiri S, et al. Recurrent R-spondin fusions in colon cancer. Nature. 2012; 488:660–664. [PubMed: 22895193]
54. O'Keefe SJ, Tamura J, Kincaid RL, Tocci MJ, O'Neill EA. FK-506– and CsA-sensitive activation of the interleukin-2 promoter by calcineurin. Nature. 1992; 357:692–694. [PubMed: 1377361]
55. Sears CL, Garrett WS. Microbes, microbiota and colon cancer. Cell Host Microbe. 2014; 15:317–328. [PubMed: 24629338]
56. Tjalsma H, Boleij A, Marchesi JR, Dutilh BE. A bacterial driver-passenger model for colorectal cancer: beyond the usual suspects. Nat Rev Microbiol. 2012; 10:575–582. [PubMed: 22728587]
57. Wu S, et al. A human colonic commensal promotes colon tumorigenesis via activation of T helper type 17 T cell responses. Nat Med. 2009; 15:1016–1022. [PubMed: 19701202]
58. Anderson MJ, Willis TJ. Canonical analysis of principal coordinates: a useful method of constrained ordination for ecology. Ecology. 2003; 84:511–525.
59. Benjamini Y, Hochberg Y. Controlling the false-discovery rate: a practical and powerful approach to multiple testing. J R Stat Soc Series B Stat Methodol. 1995; 57:289–300.
60. Günther C, et al. Caspase-8 controls the gut response to microbial challenges by TNF-α–dependent and independent pathways. Gut. 2015; 64:601–610. [PubMed: 25379949]
61. Neal MD, et al. Toll-like receptor 4 is expressed on intestinal stem cells and regulates their proliferation and apoptosis via the p53 upregulated modulator of apoptosis. J Biol Chem. 2012; 287:37296–37308. [PubMed: 22955282]
62. Dupont A, et al. Intestinal mucus affinity and biological activity of an orally administered antibacterial and anti-inflammatory peptide. Gut. 2015; 64:222–232. [PubMed: 24811998]
63. Marchesi JR, et al. Toward the human colorectal cancer microbiome. PLoS One. 2011; 6:e20447. [PubMed: 21647227]
64. Neilson JR, Winslow MM, Hur EM, Crabtree GR. Calcineurin B1 is essential for positive but not negative selection during thymocyte development. Immunity. 2004; 20:255–266. [PubMed: 15030770]
65. Aliprantis AO, et al. NFATc1 in mice represses osteoprotegerin during osteoclastogenesis and dissociates systemic osteopenia from inflammation in cherubism. J Clin Invest. 2008; 118:3775–3789. [PubMed: 18846253]
66. Canté-Barrett K, Winslow MM, Crabtree GR. Selective role of NFATc3 in positive selection of thymocytes. J Immunol. 2007; 179:103–110. [PubMed: 17579027]
67. Madison BB, et al. Cis elements of the villin gene control expression in restricted domains of the vertical (crypt) and horizontal (duodenum, cecum) axes of the intestine. J Biol Chem. 2002; 277:33275–33283. [PubMed: 12065599]
68. el Marjou F, et al. Tissue-specific and inducible Cre-mediated recombination in the gut epithelium. Genesis. 2004; 39:186–193. [PubMed: 15282745]

69. Adachi O, et al. Targeted disruption of the *Myd88* gene results in loss of IL-1– and IL-18–mediated function. Immunity. 1998; 9:143–150. [PubMed: 9697844]
70. Heijmans J, et al. Rage signaling promotes intestinal tumorigenesis. Oncogene. 2013; 32:1202–1206. [PubMed: 22469986]
71. Adolph TE, et al. Paneth cells as a site of origin for intestinal inflammation. Nature. 2013; 503:272–276. [PubMed: 24089213]
72. Wirtz S, Neufert C, Weigmann B, Neurath MF. Chemically induced mouse models of intestinal inflammation. Nat Protoc. 2007; 2:541–546. [PubMed: 17406617]
73. Hill DA, et al. Metagenomic analyses reveal antibiotic-induced temporal and spatial changes in intestinal microbiota with associated alterations in immune cell homeostasis. Mucosal Immunol. 2010; 3:148–158. [PubMed: 19940845]
74. Molkentin JD, et al. A calcineurin-dependent transcriptional pathway for cardiac hypertrophy. Cell. 1998; 93:215–228. [PubMed: 9568714]
75. Wilkins BJ, et al. Calcineurin-NFAT coupling participates in pathological, but not physiological, cardiac hypertrophy. Circ Res. 2004; 94:110–118. [PubMed: 14656927]
76. De Windt LJ, et al. Calcineurin-mediated hypertrophy protects cardiomyocytes from apoptosis *in vitro* and *in vivo*: an apoptosis-independent model of dilated heart failure. Circ Res. 2000; 86:255–263. [PubMed: 10679475]
77. Sama MA, et al. Interleukin-1β–dependent signaling between astrocytes and neurons depends critically on astrocytic calcineurin-NFAT activity. J Biol Chem. 2008; 283:21953–21964. [PubMed: 18541537]
78. Zeissig S, et al. Hepatitis B virus–induced lipid alterations contribute to natural killer T cell–dependent protective immunity. Nat Med. 2012; 18:1060–1068. [PubMed: 22706385]
79. Sato T, et al. Single Lgr5 stem cells build crypt-villus structures *in vitro* without a mesenchymal niche. Nature. 2009; 459:262–265. [PubMed: 19329995]
80. D'Abaco GM, Whitehead RH, Burgess AW. Synergy between *Apc*min and an activated *ras* mutation is sufficient to induce colon carcinomas. Mol Cell Biol. 1996; 16:884–891. [PubMed: 8622690]
81. Vidal K, Grosjean I, evillard JP, Gespach C, Kaiserlian D. Immortalization of mouse intestinal epithelial cells by the SV40 large T gene. Phenotypic and immune characterization of the MODE-K cell line. J Immunol Methods. 1993; 166:63–73. [PubMed: 7693823]
82. Zeissig S, et al. Butyrate induces intestinal sodium absorption via Sp3-mediated transcriptional upregulation of epithelial sodium channels. Gastroenterology. 2007; 132:236–248. [PubMed: 17241874]
83. Macián F, García-Rodríguez C, Rao A. Gene expression elicited by NFAT in the presence or absence of cooperative recruitment of Fos and Jun. EMBO J. 2000; 19:4783–4795. [PubMed: 10970869]
84. Veeman MT, Slusarski DC, Kaykas A, Louie SH, Moon RT. Zebrafish prickle, a modulator of noncanonical Wnt-Fz signaling, regulates gastrulation movements. Curr Biol. 2003; 13:680–685. [PubMed: 12699626]
85. Zeissig S, et al. Primary deficiency of microsomal triglyceride transfer protein in human abetalipoproteinemia is associated with loss of CD1 function. J Clin Invest. 2010; 120:2889–2899. [PubMed: 20592474]
86. Rehman A, et al. Transcriptional activity of the dominant gut mucosal microbiota in chronic inflammatory bowel disease patients. J Med Microbiol. 2010; 59:1114–1122. [PubMed: 20522625]
87. Kozich JJ, Westcott SL, Baxter NT, Highlander SK, Schloss PD. Development of a dual-index sequencing strategy and curation pipeline for analyzing amplicon sequence data on the MiSeq Illumina sequencing platform. Appl Environ Microbiol. 2013; 79:5112–5120. [PubMed: 23793624]
88. Magoč T, Salzberg SL. FLASH: fast length adjustment of short reads to improve genome assemblies. Bioinformatics. 2011; 27:2957–2963. [PubMed: 21903629]
89. Edgar RC. UPARSE: highly accurate OTU sequences from microbial amplicon reads. Nat Methods. 2013; 10:996–998. [PubMed: 23955772]

90. Wang Q, Garrity GM, Tiedje JM, Cole JR. Naive Bayesian classifier for rapid assignment of rRNA sequences into the new bacterial taxonomy. Appl Environ Microbiol. 2007; 73:5261–5267. [PubMed: 17586664]

91. Edgar RC. Search and clustering orders of magnitude faster than BLAST. Bioinformatics. 2010; 26:2460–2461. [PubMed: 20709691]

92. Dixon P. VEGAN, a package of R functions for community ecology. J Veg Sci. 2003; 14:927–930.

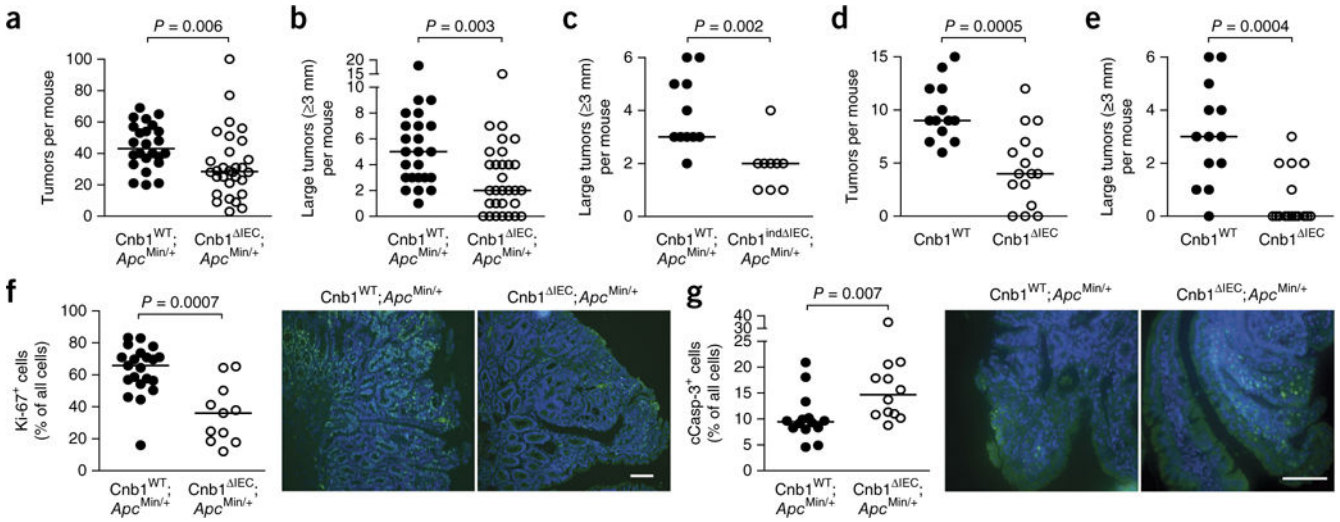

Figure 1.

Intestinal epithelial calcineurin promotes intestinal tumor development. (**a–e**) Number of total (**a,d**) and large (**b,c,e**) tumors in the small intestine of 18-week-old Cnb1$^{\Delta IEC}$;*Apc*$^{Min/+}$ (n = 30) and Cnb1^{WT};*Apc*$^{Min/+}$ (n = 24) littermates (**a,b**), the small intestine of 18-week-old Cnb1^{indΔIEC};*Apc*$^{Min/+}$ (n = 9) and Cnb1^{WT};*Apc*$^{Min/+}$ (n = 11) littermates after tamoxifen treatment (**c**), and the large intestine of Cnb1$^{\Delta IEC}$ (n = 16) and Cnb1^{WT} (n = 13) mice in the AOM-DSS model (**d,e**). (**f,g**) Quantification of cells staining positive for Ki-67 (**f**, left) or cleaved caspase-3 (cCasp-3) (**g**, left), using immunofluorescence, and representative images showing staining for Ki-67 (green) (**f**, middle and right), cCasp-3 (green) (**g**, middle and right) and DAPI (blue) in tumors from the small intestines of 18-week-old Cnb1^{WT};*Apc*$^{Min/+}$ (middle; n = 21 for Ki-67; n = 14 for cCasp-3) and Cnb1$^{\Delta IEC}$;*Apc*$^{Min/+}$ (right; n = 11 for Ki-67; n = 12 for cCasp-3) mice. Scale bars, 100 μm. The combined results of two (**d,e**) or three (c) independent experiments, or nine independent litters (**a,b,f,g**), are shown. In **a–g**, dots represent individual mice, and bar indicates median. *P* values were calculated using the Mann-Whitney *U*-test.

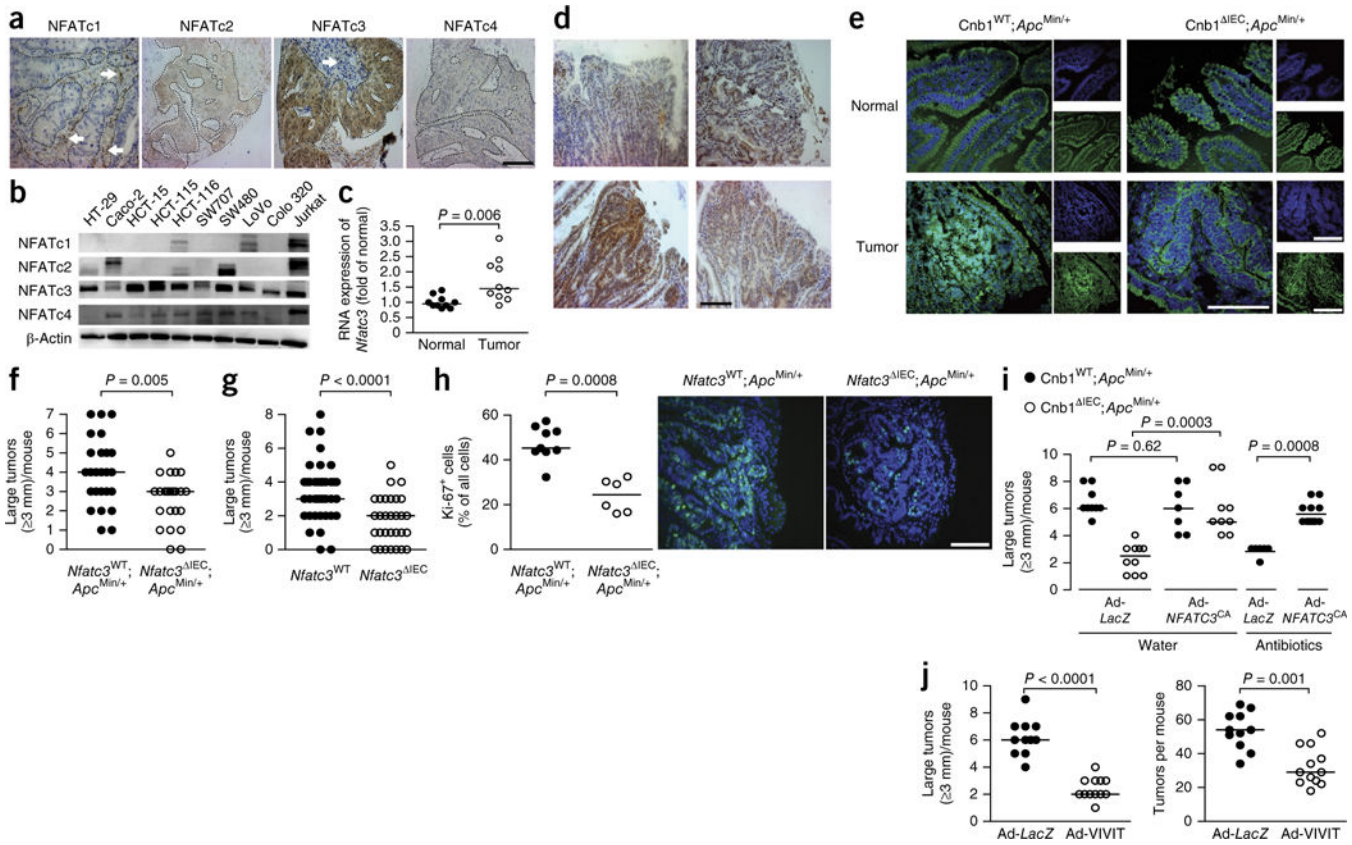

Figure 2.

Calcineurin regulates tumor development through NFAT. (**a**) Representative images showing staining of the indicated NFAT family members in samples from humans with CRC (NFATc1, $n = 28$; NFATc2, $n = 28$; NFATc3, $n = 704$; NFATc4, $n = 28$). Arrows indicate tumor-infiltrating cells, which are delineated from tumors by dashed lines. Scale bar, 100 μm. (**b**) Representative western blot analysis (of two independent experiments) for expression of NFAT transcription factors in human CRC cell lines. β-actin was used as a loading control. (**c**) qPCR analysis for *Nfatc3* expression in tumors ($n = 10$) or normal tissue ($n = 10$) from the small intestine of $Apc^{Min/+}$ mice. (**d**) Representative immunohistochemical analysis (of three independent experiments) for expression of NFATc1 (top left), NFATc2 (top right), NFATc3 (bottom left) and NFATc4 (bottom right) in tumors from the small intestine of $Apc^{Min/+}$ mice. Scale bar, 100 μm. (**e**) Representative immunofluorescence analysis (of three independent experiments) of NFATc3 (green) and DAPI (blue) in the normal mucosa (top) or tumors (bottom) of the small intestine of $Cnb1^{WT};Apc^{Min/+}$ (left) or $Cnb1^{\Delta IEC};Apc^{Min/+}$ (right) mice. Large image on the left is a merged, magnified view of the smaller images on the right. Scale bars, 100 μm. (**f,g**) Number of large tumors in the small intestine of 18-week-old $Nfatc3^{\Delta IEC};Apc^{Min/+}$ ($n = 23$) and $Nfatc3^{WT};Apc^{Min/+}$ ($n = 25$) mice (**f**) or in the large intestine of AOM-DSS-treated $Nfatc3^{\Delta IEC}$ ($n = 30$) and $Nfatc3^{WT}$ ($n = 39$) mice (**g**). (**h**) Quantification of $Ki\text{-}67^{+}$ cells (left) and representative images for Ki-67 (green) and DAPI (blue) staining (middle and right) in tumors from the small intestine of $Nfatc3^{WT};Apc^{Min/+}$ ($n = 9$, middle) and $Nfatc3^{\Delta IEC};Apc^{Min/+}$ ($n = 6$, right) mice. Scale bar, 100 μm. (**i,j**) Number of large (**i,j**, left) or total (**j**, right) tumors in the small intestine of

Cnb1^{WT};*Apc*$^{Min/+}$ mice and Cnb1$^{\Delta IEC}$;*Apc*$^{Min/+}$ littermates after administration of Ad-*NFATC3*^{CA} or Ad-*LacZ*, with (Ad-*LacZ*: Cnb1^{WT};*Apc*$^{Min/+}$, $n = 6$; Ad-*NFATC3*^{CA}: Cnb1^{WT};*Apc*$^{Min/+}$, $n = 10$) or without (Ad-*LacZ*: Cnb1^{WT};*Apc*$^{Min/+}$, $n = 9$; Cnb1$^{\Delta IEC}$;*Apc*$^{Min/+}$, $n = 10$; Ad-*NFATC3*^{CA}: Cnb1^{WT};*Apc*$^{Min/+}$, $n = 7$; Cnb1$^{\Delta IEC}$;*Apc*$^{Min/+}$, $n = 9$) antibiotics (**i**; see Online Methods), or of Cnb1^{WT};*Apc*$^{Min/+}$ mice after administration of Ad-*LacZ* ($n = 11$ per group) or Ad-VIVIT ($n = 12$ per group) (**j**). In **g,i,j**, combined data for three (**g**), four (**j**) and six (**i**) independent experiments are shown. In all graphs, dots represent individual mice, and bar indicates median. *P* values were calculated using the Mann-Whitney *U*-test.

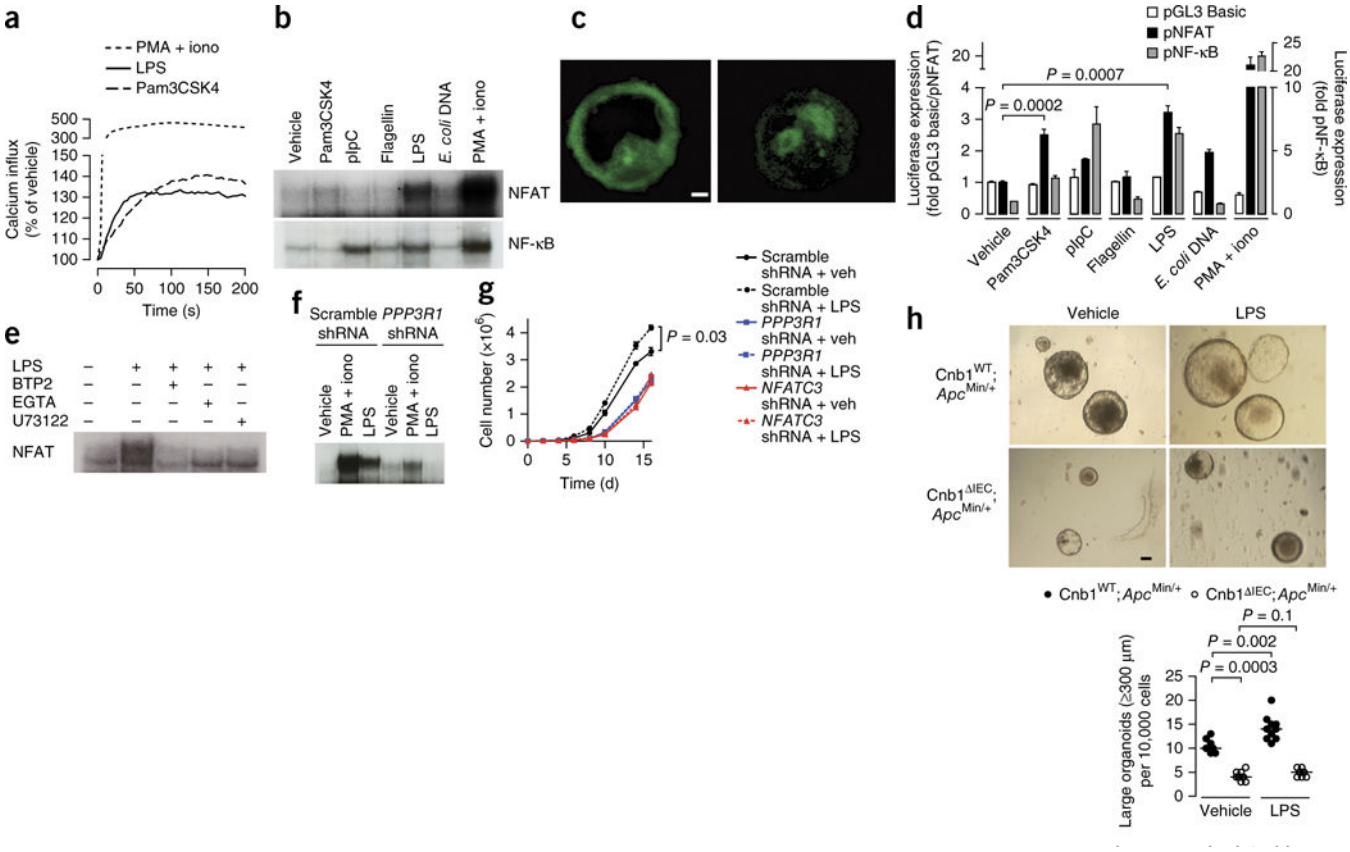

Figure 3.

TLR stimulation promotes NFAT activation in CRC. (**a,b**) Representative calcium flux analysis (**a**) and electrophoretic mobility shift assays (EMSAs) for NFAT and/or NF-κB DNA-binding activity (**b**) in SW707 human CRC cells in response to agonists of TLR2 (Pam3CSK4), TLR3 (polyinosinic-polycytidylic acid; pIpC), TLR4 (LPS), TLR5 (flagellin) and TLR9 (*Escherichia coli* DNA). Treatment with PMA + ionomycin (iono) was used as a control. (**c**) Representative images of live-cell tracking analysis for ectopically expressed NFATc3–GFP in SW707 cells before (left) and 20 min after (right) LPS treatment. Scale bar, 1 μm. (**d**) Firefly luciferase expression, normalized to control *Renilla* luciferase expression, in SW707 cells after transfection of NFAT- or NF-κB–dependent luciferase reporter plasmids and in response to the indicated TLR agonists ($n = 3$ cultures per condition). Data are mean ± s.e.m. *P* values were calculated by one-way analysis of variance (ANOVA) followed by Dunnett's test. (**e,f**) Representative EMSA analysis for NFAT DNA-binding activity in nuclear fractions of SW707 cells (**e**) or SW707 cells stably expressing a *PPP3R1*-specific shRNA or a nontargeting control (scramble) shRNA (**f**). (**g**) Time course for proliferation of SW707 cells stably expressing a *PPP3R1*-specific or *NFATC3*-specific shRNA, or a nontargeting control (scramble) shRNA, in the presence of LPS or vehicle (veh) ($n = 3$ cultures per condition). Data are mean ± s.e.m. *P* value was calculated by Student's *t*-test. (**h**) Representative images (left and right) and quantification (bottom) of large organoids obtained from tumors of $Cnb1^{\Delta IEC};Apc^{Min/+}$ (vehicle-treated, $n = 10$; LPS-treated, $n = 9$) and $Cnb1^{WT};Apc^{Min/+}$ mice (vehicle-treated, $n = 9$; LPS-treated, $n = 10$) after *in vitro* treatment with vehicle or LPS for 7 d. Circles in graph indicate individual organoid

cultures, and the bar indicates median. Scale bar, 100 μm. *P* values were calculated by the Kruskal-Wallis test followed by Dunn's test. Data in a–h are representative of three independent experiments.

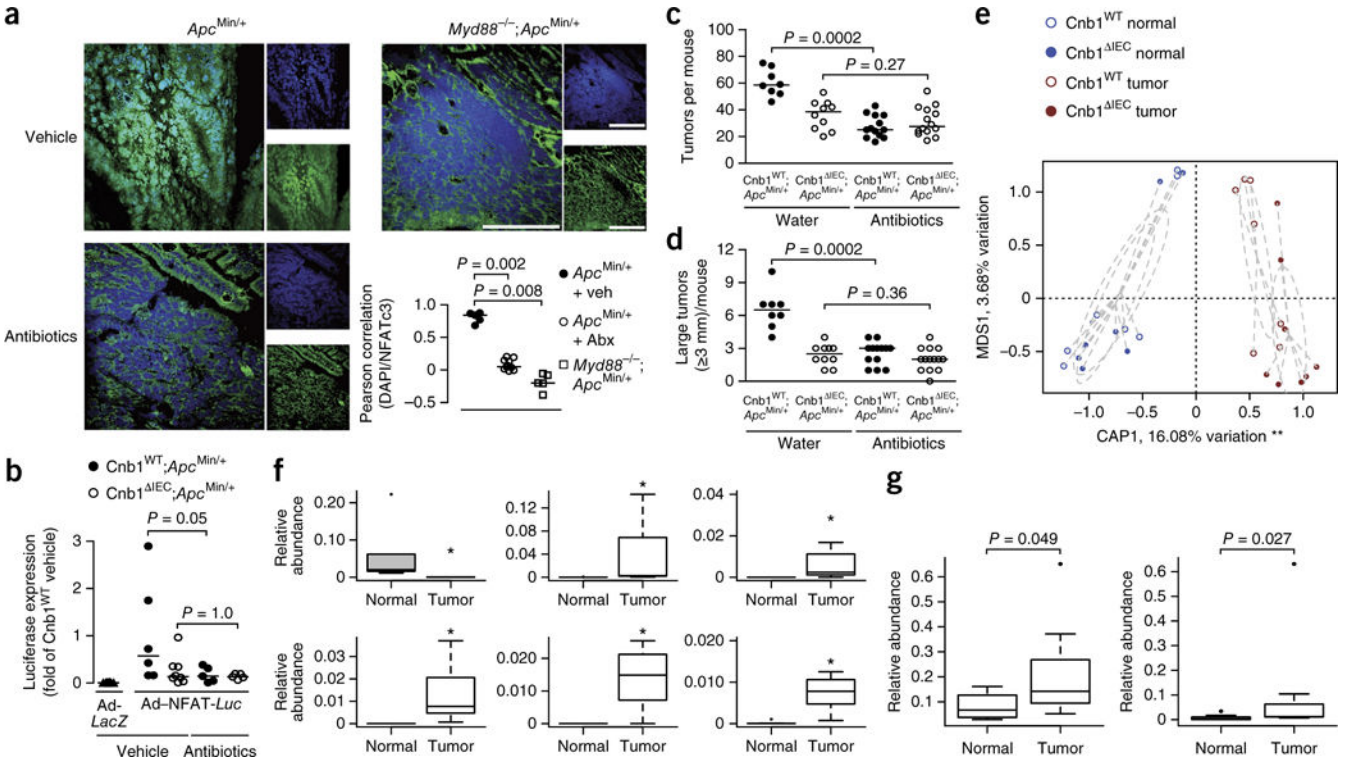

Figure 4.

Calcineurin-mediated tumor development is dependent on the microbiota. (**a**) Representative immunofluorescence images (of three independent experiments) for NFATc3 (green) and DAPI (blue) in tumors of the small intestine of $Apc^{Min/+}$ mice (left) that were treated with vehicle (veh) (top left) or antibiotics (Abx) (bottom left) and $Myd88^{-/-}$;$Apc^{Min/+}$ mice (top right). Bottom right, quantification of NFATc3 nuclear translocation using the Pearson correlation coefficient in $Apc^{Min/+}$ mice treated with vehicle ($n = 5$) or Abx ($n = 11$), and in $Myd88^{-/-}$;$Apc^{Min/+}$ mice ($n = 5$). *P* values were calculated by the Kruskal-Wallis test followed by Dunn's test. Scale bars, 100 μm. (**b**) Luciferase expression, normalized to protein concentration, in tumors in the small intestine of Cnb1^{WT};$Apc^{Min/+}$ mice administered Ad-*LacZ* ($n = 8$) or Ad–NFAT-*Luc* and treated with water (vehicle, $n = 6$) or antibiotics ($n = 5$), and in the small intestine of Cnb1$^{\Delta IEC}$;$Apc^{Min/+}$ mice treated with water ($n = 8$) or antibiotics ($n = 5$) for 14 weeks (Online Methods). (**c,d**) Quantification of total (**c**) and large (**d**) tumors in the small intestine of Cnb1^{WT};$Apc^{Min/+}$ mice after treatment with antibiotics ($n = 13$) or vehicle ($n = 8$), and in the small intestine of Cnb1$^{\Delta IEC}$;$Apc^{Min/+}$ mice after treatment with antibiotics ($n = 14$) or vehicle ($n = 10$) for 14 weeks. In a–d, bar indicates the median, and dots represent individual mice. Combined results of two (**a,b**) or four (**c,d**) independent experiments are shown. *P* values in b–d were calculated by the Mann-Whitney *U*-test. (**e**) Constrained analysis of principle coordinates ('capscale'; CAP)58 based on Bray-Curtis distances for Cnb1^{WT};$Apc^{Min/+}$ mice ($n = 7$ for normal and tumor) and Cnb1$^{\Delta IEC}$;$Apc^{Min/+}$ mice ($n = 8$ for normal and tumor). CAP1 separates normal intestinal mucosa (blue) and tumors (brown; double asterisk indicates adonis $P = 0.003$) but not genotypes (filled dots and circles; $P > 0.05$ in analysis of dissimilarity, 'adonis'); MDS1 represents first nonconstrained axis after controlling the effect of tissues. (**f**) Species-level

OTUs with differences between normal ($n = 7$) and tumor tissue ($n = 7$) of $Apc^{Min/+}$ mice. The six OTUs with significant differences (Wilcoxon test $P < 0.05$ after correction for multiple testing[59]) that were identified among the major OTUs (average relative abundance >0.5%) comprise *Prevotella* (top left), *Lactobacillus* (top middle), *Escherichia* and *Shigella* (top right), *Tannerella* (bottom left), *Parabacteroides* (bottom middle) and *Citrobacter* (bottom right). $*P < 0.05$; by the Wilcoxon test, after correction for multiple testing; boxes represent the 50% confidence interval; error bars represent the 95% confidence interval of the relative abundance, with the line in the box representing the mean value. (**g**) Relative abundance of Proteobacteria (left) and *Enterobacteriaceae* (right) in normal ($n = 7$) and tumor tissue ($n = 7$) of $Apc^{Min/+}$ mice. Matched normal and tumor mucosa are shown in e–g.

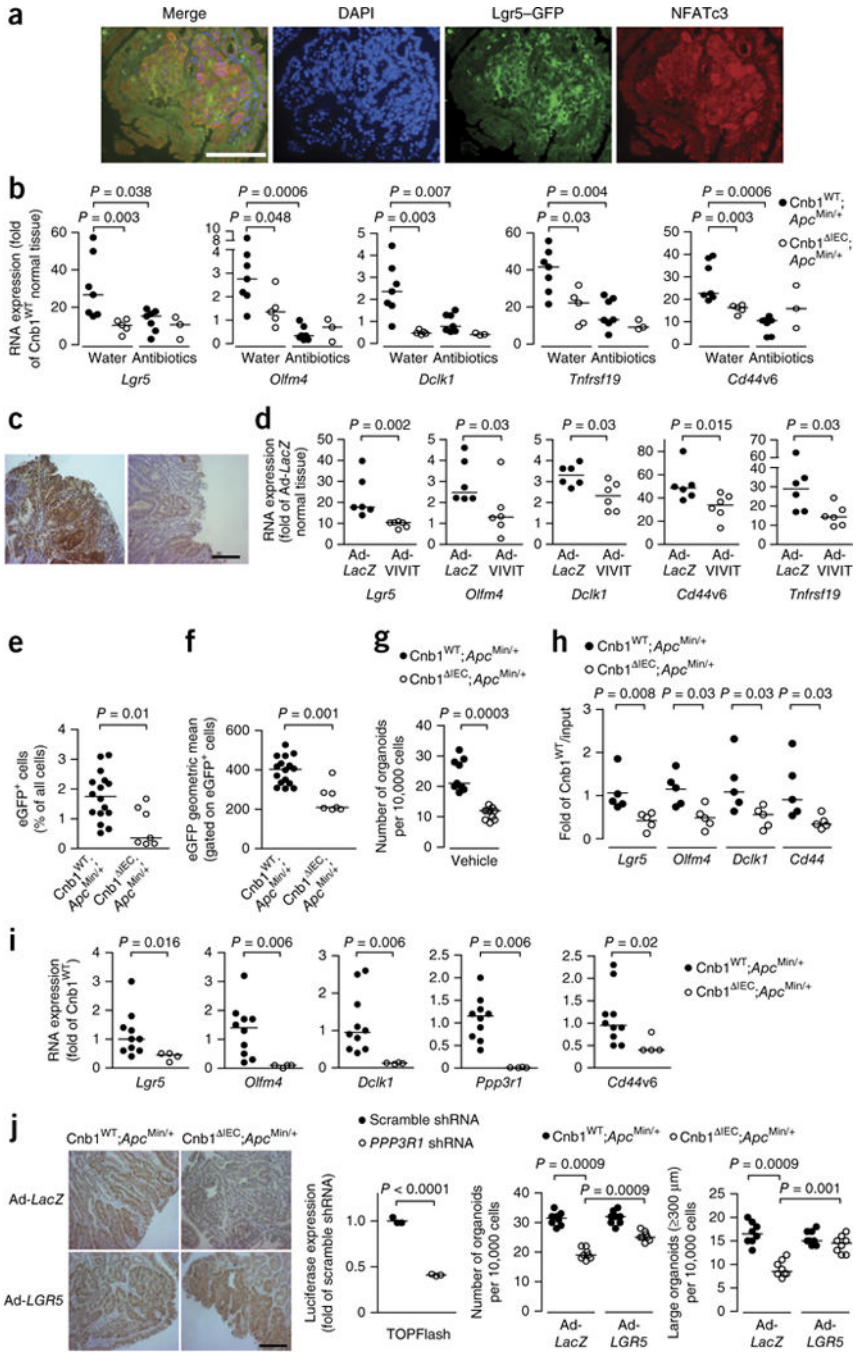

Figure 5.

Calcineurin and NFATc3 regulate cancer stem cells. (**a**) Representative immunofluorescence images (of three independent experiments) for NFATc3 (red), Lgr5–eGFP (green) and DAPI (blue) in tumors from *Lgr5-EGFP*-IRES-CreERT2;$Apc^{Min/+}$ mice. Scale bar, 100 µm. (**b**) qPCR analysis for expression of the indicated genes in intestinal tumors from $Cnb1^{WT}$;$Apc^{Min/+}$ without ($n = 7$) or with antibiotics ($n = 7$) and from $Cnb1^{\Delta IEC}$;$Apc^{Min/+}$ mice without ($n = 5$) or with antibiotics ($n = 3$). (**c**) Representative immunohistochemistry images (of three independent experiments) for DCLK1 in intestinal tumors from

Cnb1^{WT};*Apc*$^{Min/+}$ (left) and Cnb1$^{\Delta IEC}$;*Apc*$^{Min/+}$ (right) mice. Scale bar, 100 μm. (**d**) qPCR analysis for the expression of the indicated genes in intestinal tumors from *Apc*$^{Min/+}$ mice after administration of Ad-*LacZ* (n = 6) or Ad-VIVIT (n = 6) (Online Methods). (**e,f**) Relative numbers of eGFP^{+} cells (**e**) or the geometric mean of eGFP expression among gated eGFP^{+} cells (**f**) in intestinal tumors from Cnb1$^{\Delta IEC}$;*Apc*$^{Min/+}$ (n = 7) and Cnb1^{WT};*Apc*$^{Min/+}$ littermates (n = 16) on the *Lgr5-EGFP*-IRES-CreER^{T2} background. (**g**) Quantification of organoids derived from tumors of Cnb1^{WT};*Apc*$^{Min/+}$ (n = 9) and Cnb1$^{\Delta IEC}$;*Apc*$^{Min/+}$ mice (n = 10). (**h**) qPCR analysis for expression of the indicated genes after NFATc3 ChIP in intestinal tumors from Cnb1^{WT};*Apc*$^{Min/+}$ (n = 5) and Cnb1$^{\Delta IEC}$;*Apc*$^{Min/+}$ mice (n = 5). (**i**) qPCR analysis for expression of the indicated genes in sorted eGFP^{+} cells from intestinal tumors from Cnb1^{WT};*Apc*$^{Min/+}$ (n = 10) and Cnb1$^{\Delta IEC}$;*Apc*$^{Min/+}$ mice (n = 4) that were on the *Lgr5-EGFP*-IRES-CreER^{T2} background. (**j**) Representative immunohistochemistry images of β-catenin in intestinal tumors from Cnb1^{WT};*Apc*$^{Min/+}$ (left) and Cnb1$^{\Delta IEC}$;*Apc*$^{Min/+}$ (right) mice after administration of Ad-*LacZ* (top) or Ad-*LGR5* (bottom) (Online Methods). Left graph shows normalized expression of firefly luciferase after transfection of a TCF- and LEF-dependent firefly luciferase construct and a control *Renilla* luciferase construct into SW707 cells stably expressing a *PPP3R1*-specific shRNA (n = 3) or a nontargeting control (scramble) shRNA (n = 3). Middle and right graphs show the number of total (middle) or large (right) organoids derived from tumors of Ad-*LacZ*–treated or Ad-*LGR5*–treated Cnb1$^{\Delta IEC}$;*Apc*$^{Min/+}$ and Cnb1^{WT};*Apc*$^{Min/+}$ littermates (n = 8 per group). Scale bar, 100 μm. Combined results of two (**d–f,i**) or three (**b,h**) independent experiments, or results representative of three independent experiments (**a,c,g,j**), are shown, with dots representing individual mice (**b,d–f,h,i**), organoid cultures (**g,j** middle and right graphs) or triplicate cultures (**j**, left graph). Bar indicates the mean (**j** left graph) or median (**b,d–j**, middle and right graphs). The Mann-Whitney *U*-test (**d–i**), the Student's *t*-test (**j**, left graph) or the Kruskal-Wallis test followed by Dunn's test (**b,j** middle and right graphs) was used to calculate *P* values.

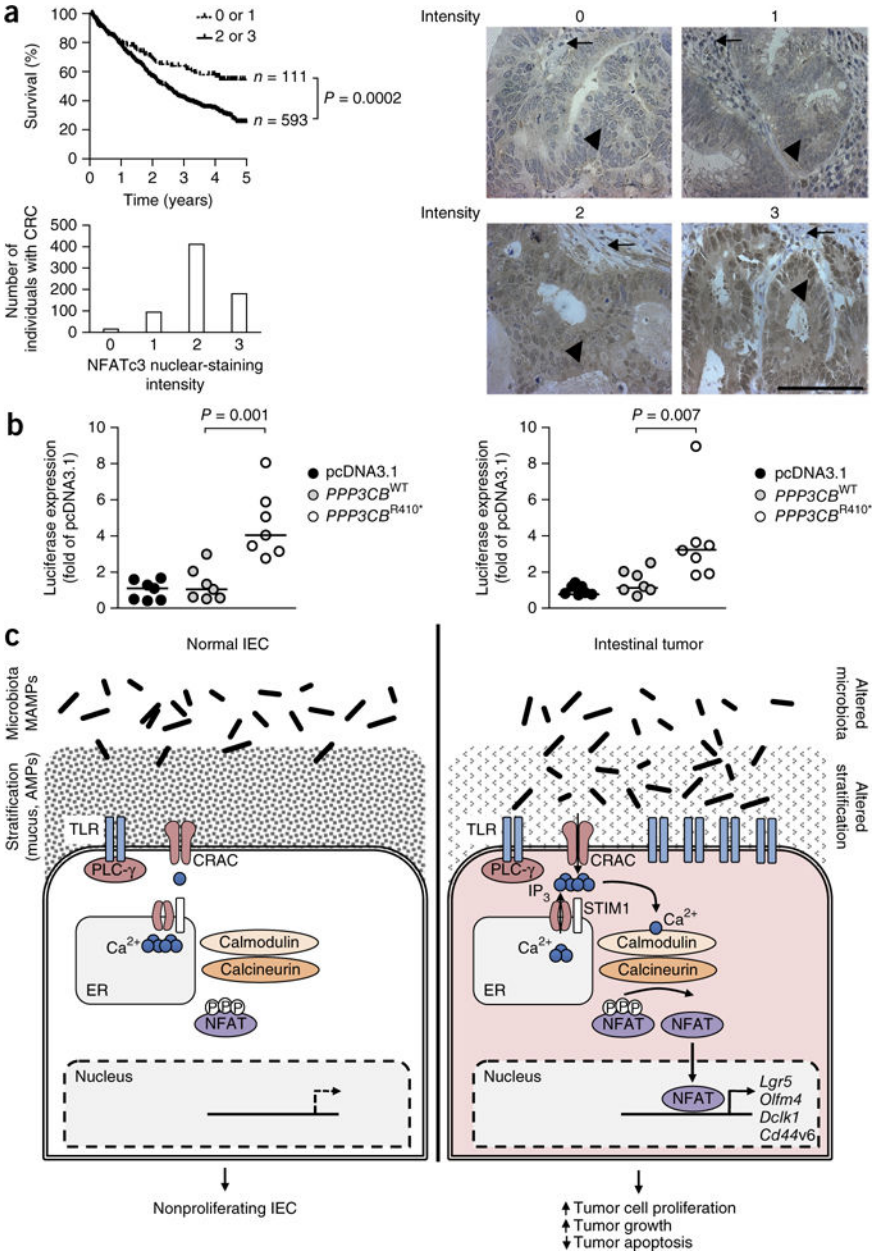

Figure 6.

Activation of NFATc3 is associated with increased death from CRC. (**a**) Top left: Kaplan-Meier analysis of the survival (death from CRC) of individuals with CRC, plotted according to the nuclear staining intensity of NFATc3 in CRC tissue. Right: representative immunohistochemistry images of nuclear NFATc3 staining and scoring. Bottom left, quantification of CRC tissues according to the intensity of NFATc3 nuclear staining (0 (*n* = 16), 1 (*n* = 95), 2 (*n* = 412) or 3 (*n* = 181)). Arrows indicate stromal cells; arrowheads indicate tumor cells. Scale bar, 100 μm. The *P* value was calculated by the log-rank test. (**b**) Firefly luciferase expression, normalized to that of *Renilla* luciferase, after transfection of an NFAT-dependent firefly luciferase construct and either constructs expressing WT or mutant CnA-β or the empty plasmid (pcDNA3.1) into SW707 cells that were stably expressing a

PPP3R1-specific shRNA (right) or a nontargeting control shRNA (left) ($n = 7$ per group). Dots represent individual cell cultures. Bar indicates the median. *P* values were calculated by the Mann-Whitney *U*-test. The results are representative of three independent experiments. (**c**) Schematic summary. In normal epithelium (left), limited TLR expression[60,61] and separation of the luminal microbiota from IECs[62] prevents microbiota-induced calcineurin-dependent NFAT signaling. In intestinal tumors (right), increased TLR expression36, dysbiosis[23,25,63] and impaired stratification of the luminal microbiota[5,25] allows for TLR-dependent, store-operated calcium entry via calcium release activated channels (CRACs). This leads to calcium-dependent calcineurin activation and NFAT-dependent transcription of stem cell–associated genes, which promote tumor proliferation and prevent apoptosis. AMPs, antimicrobial peptides; ER, endoplasmic reticulum; PLC-γ, phospholipase C gamma; MAMPs, microbe-associated molecular patterns; STIM1, stromal interaction molecule 1; IP_3, inositol 1,4,5-trisphosphate.